Effects of spatial variability on the exposure of fish to hypoxia: a modeling analysis for the Gulf of Mexico

Elizabeth D. LaBone[1], Kenneth A. Rose[2], Dubravko Justic[1], Haosheng Huang[1], and Lixia Wang[1]

[1]Department of Oceanography and Coastal Sciences, Louisiana State University, Baton Rouge, LA, USA
[2]University of Maryland Center for Environmental Science, Horn Point Laboratory, Cambridge, MD, USA
Correspondence: Elizabeth D LaBone (elabon1@lsu.edu)

Abstract. The hypoxic zone in the northern Gulf of Mexico varies spatially (area, location) and temporally (onset, duration) on multiple scales. Exposure to hypoxic dissolved oxygen (DO) concentrations (< 2 mg L^{-1}) is often lethal and exposure to 2 to 4 mg L^{-1} often causes the sublethal effects of decreased growth and fecundity on individuals of many fish species. We simulated the movement of individual fish within a high-resolution 3-D coupled hydrodynamic-water quality model (FVCOM-

5 WASP) configured for the northern Gulf of Mexico to examine how spatial variability in DO concentrations would affect fish exposure to hypoxic and sublethal DO concentrations. Eight static snapshots (spatial maps) of DO were selected from a 10 day FVCOM-WASP simulation that showed a range of spatial variation (degree of clumpiness) in sublethal DO area from moderate total sublethal area (4 maps) to high total sublethal area (4 maps). An additional case of allowing DO to vary in time (dynamic DO) was also included. All simulations were for 10 days and were performed for 2-D (bottom layer only)

10 and 3-D (allows for vertical movement of fish) sets of maps. Fish movement was simulated every 15 minutes using one of three algorithms designed for avoiding low DO exposure and a default algorithm not dependent on DO conditions. Fish were assumed to have either good or poor avoidance competencies. Cumulative exposure of individuals to hypoxia was higher under the high sublethal area snapshots compared to the moderate sublethal area snapshots. The effects of different degrees of spatial variability on hypoxia exposure were small. Despite the differences in exposure to hypoxia with good versus poor competency,

15 both resulted in relatively high exposures to sublethal DO concentrations. Spatial variability in DO had opposite effects on sublethal exposure between moderate and high sublethal area maps: the percentage of fish exposed to 2–3 mg L^{-1} decreased with increasing variability for high sublethal area but increased for moderate sublethal area. There was a substantial inter-individual variability in exposure to hypoxic and sublethal DO that, when combined with spatial variability in DO, can result in underestimation of sublethal effects (e.g., growth) when exposure of individuals is averaged by spatial cells. By following

20 hundreds of thousands of individuals over multiple generations within 3-D hydrodynamic-water quality models, we aim to predict fish population-level responses to hypoxia under management actions designed to reduce nutrient inputs.

1 Introduction

Hypoxia is expanding at locations with historical hypoxia and is appearing in new locations in the global ocean and associated
coastal waters (Breitburg et al., 2018). The hypoxic zone in the northern Gulf of Mexico (GOM) is one of the world's largest
areas (up to ~23,000 km^2) of seasonal, coastal hypoxia (Rabalais et al., 2007; Rabalais and Turner, 2019). Hypoxia is often
defined as a dissolved oxygen (DO) concentration less than 2 mg L^{-1} (Rabalais et al., 2001). In the GOM, hypoxia generally
occurs between April and October (Turner and Rabalais, 1991). The formation of hypoxia is influenced by the high river
discharges in the spring from the Mississippi and Atchafalaya rivers that bring nutrients and fresh water to the shelf that
then trigger increased primary productivity and water column stratification. The layer of fresh river water, weak tides, and
weak winds during the spring and summer, all contribute to strong stratification (Rabalais et al., 2001, 2002). Organic matter
resulting from nutrient-enhanced surface primary production sinks to the bottom layer where it is respired. Because of the
strong stratification during summertime, oxygen supply is generally lower than respiration, thus creating conditions favorable
for hypoxia development (Justic et al., 1996; Rabalais et al., 2002). Hypoxia is broken up in the fall by increased winds
associated with cold fronts and cooling of surface waters. Annual summertime (July) surveys since 1985 have documented
a highly variable hypoxic area whose extent during 1985 to 2011 varied from 700 to 23,200 km^2 (Table S2 in Obenour
et al., 2013). The areal extent of hypoxia is expected to increase under future climate change scenarios (Justic et al., 2003;
Sperna Weiland et al., 2012; Lehrter et al., 2017; Rabalais and Turner, 2019). The interannual variation in hypoxic area in the
GOM has been extensively analyzed using regression and simplified semi-empirical (e.g., box model) methods (Obenour et al.,
2015; Scavia et al., 2017; Del Giudice et al., 2019), as well as with more complex three-dimensional coupled hydrodynamic-
biogeochemical models (e.g., Fennel et al., 2013; Justić and Wang, 2014).

In addition to interannual variation, the hypoxic zone within the GOM varies spatially during the summer depending on the
interaction of various physical and biological factors, local bathymetry, wind forcing, hydrodynamics, solar radiation, river
freshwater and nutrient inputs, phytoplankton productivity, and zooplankton grazing (Bianchi et al., 2010). The hypoxic zone
typically includes a core area that is hypoxic over most summers with outer regions where DO concentrations are typically
more variable in time and space (Rabalais et al., 2007; DiMarco et al., 2010). Continuous DO measurements at fixed locations
often show rapid changes (on the order of ±1–3 mg L^{-1} h^{-1}) in bottom DO concentrations (Babin and Rabalais, 2009; Bianchi
et al., 2010; Rabalais et al., 2010; Babin, 2012). Such temporal variations have also been documented for other coastal systems
(e.g., Sanford et al., 1990; Booth et al., 2014). These temporal variations are caused by the combined effects of local DO
dynamics and the transport of DO via the movement of water and therefore imply some degree of spatial variation. Spatial
analysis of DO measured synoptically at multiple locations in the GOM shows various degrees of patchiness in hypoxia on
kilometer scales (Zhang et al., 2009), and such spatial variation is common in other estuarine systems (e.g., Muller et al., 2016).
Hypoxia in the GOM also varies in the vertical dimension. For example, the thickness of the hypoxic zone varied from less
than a meter to 20 m over the historical record (Fig. S2 in Obenour et al., 2013). Rose et al. (2018b) summarized continuous
measurements of DO obtained using a towed vehicle (Scanfish) that undulated between 2 m below the surface and 2 m above
the bottom (Roman et al., 2012; Zhang et al., 2014), and documented that bottom DO can frequently change by about 0.5 mg

L^{-1} min^{-1} on the scale of 10's of meters. It seems that the more we look, the more we find that low DO varies on increasingly finer temporal and spatial scales. Understanding these finer scales is relevant for quantifying the exposure of mobile organisms such as fish.

60   Individual fish are affected both directly and indirectly by hypoxia. Direct effects of hypoxia on fish include mortality, and the sublethal effects of reduced fecundity and growth (Shimps et al., 2005; Stierhoff et al., 2006; Rose et al., 2009; Thomas and Rahman, 2012). Fish and other organisms change their movement behavior to avoid lethal levels of DO (Eby and Crowder, 2002; Bell and Eggleston, 2005; Pollock et al., 2007; Craig, 2012). However, while many species avoid hypoxia, they are still exposed to low DO concentrations (2 to 4.5 mg L^{-1}) that cause sublethal effects (Vaquer-Sunyer and Duarte, 2009; Hrycik et al.,

65   2017). Indirect effects of hypoxia on fish include changes in mortality, growth, and fecundity that result from avoidance of low DO, causing fish to experience less suitable habitat in their new locations as well as by direct effects of low DO on their prey and predators. Hypoxia avoidance can result in fish being forced out of preferred habitat to one where there are fewer suitable prey and less shelter from predators (Eby and Crowder, 2002). Hypoxia can also affect the size, growth, energy demands, behavior of predators (Pollock et al., 2007; Breitburg et al., 2009) and the productivity, distribution, and composition of their

70   zooplankton and benthic prey (Baustian et al., 2009; Levin et al., 2009; Roman et al., 2019). While effects on individuals have been well documented in the laboratory under known and fixed exposures, major challenges remain to estimate exposure of fish to dynamically-changing DO in two and three dimensions (Rose et al., 2009; LaBone et al., 2019), and to translate these time-varying exposures to growth, mortality, and reproduction effects (Neilan and Rose, 2014).

      The fine-scale temporal and spatial dynamics of DO have been simulated in the GOM using high-resolution, three-dimensional

75   (3-D) coupled hydrodynamic-biogeochemical models (Fennel et al., 2016; Rose et al., 2017). These include the FVCOM-WASP (Finite Volume Coastal Ocean Model - Water Quality Analysis Simulation Program) model (Justić and Wang, 2014) and an implementation of the ROMS (Regional Ocean Modeling System) model coupled with a water quality and NPZ model (Fennel et al., 2013). FVCOM is an open source, unstructured grid ocean circulation model (Chen et al., 2011). WASP is a water quality model with a number of modules, including one for eutrophication (Wool et al., 2006). We have previously used

80   the FVCOM-WASP model and added the capability to simulate the fine-scale movement of individual fish (Justić and Wang, 2014; Rose et al., 2014). The same model set-up used here was previously used to compare the effects of different movement algorithms (LaBone et al., 2017) and 2-D versus 3-D avoidance movement on fish exposure to hypoxia (LaBone et al., 2019).

      In this paper, we build upon the analysis of LaBone et al. (2017, 2019) and quantify fish exposure to hypoxia and sublethal DO concentrations under different levels of spatial variability in DO on static maps. For comparison, we also include the

85   dynamic DO map from which we extracted the static maps as snapshots. Spatial variability in DO on the static maps was summarized statistically to ensure that contrasting levels of spatial variability were selected for the analysis. FVCOM-WASP was used to generate the dynamic DO fields within which the individual fish moved and experienced static or dynamic (hourly changing) DO concentrations. Movement of individual fish was modeled every 15 minutes for 10 days on the static and dynamic maps of DO within the same grid as used by FVCOM-WASP. Effects of spatial variability in DO concentrations on exposure

90   were compared for fish with poor versus good avoidance capabilities and with and without an option for vertical avoidance. The results for the 2-D (bottom layer) and 3-D (vertical avoidance allowed) analyses were similar so here we focus on the 2-D

results; the 3-D results are summarized in the Supplemental Material (https://doi.org/10.5194/bg-0-1-2020-supplement). Our overarching hypothesis was that more spatially-variable DO conditions should result in higher hypoxia (lethal) and sublethal exposures. However, our results showed that the relationship between spatial variability and exposure is complex; the effects

95 of spatial variability on sublethal exposures are highly dependent on the areal extent of sublethal DO levels.

2 Methods

2.1 FVCOM-WASP

Output from the coupled FVCOM-WASP model (Justić and Wang, 2014) was used with the FVCOM particle tracking module that was modified to simulate behavioral movement of individual fish. Individual fish were followed within the same 3-D grid

100 that was used for hydrodynamics and the water quality modeling. The model domain covered the coastal GOM from Mobile Bay, Alabama, to Galveston Bay, Texas, and extended offshore to a depth up to 300 m with the water column divided into 30 sigma layers (Fig. 1, Wang and Justic, 2009). The unstructured model grid allows higher resolution along the coast and an accurate representation of the GOM coastline. FVCOM-WASP model has been previously calibrated to accurately represent the circulation and stratification on the shelf (Wang and Justic, 2009). Hourly DO from a 10 day simulation (20–30 August

105 2002) was used as the source for the 2-D and 3-D static and dynamic DO maps. The 20-30 August 2002 time period had a large hypoxic zone (~16,000 km^2) that showed variation at fixed locations on hourly and daily time scales. The bottom sigma layer from the 3-D FVCOM-WASP model output was used to create 2-D DO maps for simulating fish movement so that the DO values in the bottom layer were identical for the 2-D and 3-D maps.

2.2 Movement algorithms

110 Fish movement was simulated within the FVCOM-WASP grid by using a suite of algorithms that determined the velocities of individual fish in the horizontal plane ($\boldsymbol{u}$ and $\boldsymbol{v}$) for 2-D and additionally the vertical velocity ($\boldsymbol{w}$) for the 3-D simulations (Rose et al., 2014; LaBone et al., 2019). The changes in fish position were calculated by updating their previous time step's positions on the grid with the newly computed velocities to obtain the new positions of the fish (Watkins and Rose, 2013; Rose et al., 2014). In 2-D, the equations are:

115 $$x(t + \Delta t) = x(t) + \boldsymbol{u}(t) \cdot \Delta t \qquad (1)$$

$$y(t + \Delta t) = y(t) + \boldsymbol{v}(t) \cdot \Delta t \qquad (2)$$

where x and y were the fish positions on the model grid (distance in meters from bottom left-hand corner of grid), $\boldsymbol{u}$ and $\boldsymbol{v}$ are the velocities in the x and y directions, and Δt is the time step (15 minutes). The velocities $\boldsymbol{u}$ and $\boldsymbol{v}$ were calculated each time

120 step as:

$$\boldsymbol{u}(t) = ss \cdot \cos(\theta(t)) \qquad (3)$$

$$\boldsymbol{v}(t) = ss \cdot \sin(\theta(t)) \tag{4}$$

where ss was the swimming speed (m sec^{-1}) and θ was the swimming angle (radians) relative to the x-axis. The swimming
125 speed and swimming angle were computed differently among the algorithms, and which algorithm to use was selected based
on the DO concentrations experienced by the fish. The collection of algorithms to model fish movement and exposure to DO
were the same as used in previous analyses (LaBone et al., 2017, 2019).

2.2.1   Event-based movement

An event-based algorithm was used to choose among the various algorithms that computed swim speed and angle. There were
130 four possible algorithms that an individual fish could use on a time step: neighborhood search (NS), Sprint, correlated random
walk (CRW), and Cauchy CRW (CCRW). On each time step, two cues for DO-related movement were computed (e1 and e2),
and these were used to select among three avoidance algorithms (NS, Sprint, and CRW) depending on the severity of hypoxia
exposure. When none of the three DO-related algorithms for avoidance were selected, the individual used the default movement
algorithm (CCRW) that was unrelated to DO conditions. The cuing variables e1 and e2 were binary variables (zero or one)
135 computed on each time step (every 15 minutes) for each individual, with e1 being triggered when the DO concentration in the
cell (exposure now) was less than 2 mg L^{-1} and e2 was triggered when an individual's cumulative exposure to DO < 2 mg L^{-1}
exceeded a continuous 48 hours. Thus, each individual had its own evolving time series of zero or one values for each cue (e1
and e2).

2.2.2   Neighborhood search

140 When the NS algorithm was selected by the event-based algorithm it was considered a tactical (immediate and urgent) response
because the individual fish was about to be exposed to DO < 2 mg L^{-1}. The individual then searched the surrounding cells for
the one with the lowest DO value and moved in the opposite direction at a swim speed twice the baseline (default) speed. The
angle and swimming speed were calculated as:

$$\theta(t) = \text{atan2}(y(t) - yl(t), x(t) - xl(t)) + 0.15 \cdot 2\pi(2 \cdot ran - 1) \tag{5}$$

145

$$ss = 2 \cdot ss_0 \pm ss_0 \cdot ran \tag{6}$$

where x(t) and y(t) are the current x and y coordinates, xl(t) and yl(t) are the coordinates of the center of the cell with the lowest
DO, ss_0 is the default swim speed, and ran is a uniform random number. The first part of Eq. (5) (atan2( )), calculates the angle
and the second part of the equation calculates a random component that adds some variability to the angle. The NS algorithm is
150 efficient at avoiding hypoxia, but fish could get stuck in local maxima that were still hypoxic. The random component added to
the swimming angle prevented most, but not all, fish from getting stuck at local hypoxic cells that were also the local maximum
DO concentration.

2.2.3 Sprint

The Sprint algorithm was also considered a tactical response to hypoxia exposure and was selected when an individual fish
155 spent too long in the hypoxic waters, often the result of being stuck at local hypoxic maxima from which the NS algorithm
could not successfully move fish to non-hypoxic waters. If the fish spent more than 48 continuous hours in hypoxic conditions,
the fish would swim quickly (3 times the default speed) in a straight line out of the hypoxic zone going in the direction the fish
last traveled. The angle and swimming speed were calculated as:

$$\theta(t) = \theta(t-\Delta t) \tag{7}$$

160

$$ss = 3 \cdot ss_0 \tag{8}$$

The fish used Sprint on successive time steps until it exited the hypoxic zone, when its continuous exposure to hypoxia was
reset back to zero.

2.2.4 CRW

165 CRW was a biased random walk algorithm (Kareiva and Shigesada, 1983) used for a strategic response to hypoxia. A strategic
response is considered a response to hypoxia exposure but when the exposure is not immediate (like with tactical), but rather
had occurred in the recent past. CRW, as a strategic response, typically followed the tactical NS response because once the
immediate threat of exposure was gone, there was still some memory of the immediate exposure and the individual was likely
in an area where there was hypoxia. The CRW algorithm had fish continue to swim away (at the relatively slower default speed)
170 from hypoxic areas after NS enabled the fish to exit hypoxic conditions. CRW used the velocities from the previous time step
to calculate the angle and calculated a random speed:

$$\theta(t) = \mathrm{atan2}(\boldsymbol{v}(t-\Delta t), \boldsymbol{u}(t-\Delta t)) + 0.05 \cdot 2\pi \cdot (2 \cdot ran - 1) \tag{9}$$

$$ss = ss_0 \pm 0.3 \cdot ss_0 \cdot ran \tag{10}$$

175 The first half of Eq. (9) (atan2( )), are the velocities from the previous time step and the second part of the equation is a random
component to add variation to the angle.

2.2.5 Default

CCRW was the random walk algorithm used as a default movement in the model and is a more complicated biased random
walk than CRW (Wu et al., 2000). The magnitude and direction of the bias can be controlled by choosing the turning angle
180 from a non-uniform, wrapped Cauchy distribution. The turning angle and swimming speed were calculated by:

$$\theta(t) = \theta(t - \Delta t) + 2 \cdot \mathrm{atan}\left[\frac{(1-\epsilon)}{(1+\epsilon)} \cdot \tan((ran - 0.5) \cdot \pi) \right] + \theta_m \tag{11}$$

$$ss = ss_0 \pm 0.3 \cdot ss_0 \cdot ran \tag{12}$$

where ϵ determines the shape of the wrapped Cauchy distribution and θ_m determines the center of the distribution. $\theta(t\text{-}\Delta t)$ is the previous angle and the $2*atan[\ ] + \theta_m$ is the turning angle. Higher values of ϵ result in more correlation and less randomness to the direction of the fish. The value assigned to θ_m determined the bias in whether the individual tended to turn left or right.

2.2.6 Reflective boundary

Reflective boundary was an application of the NS algorithm used to reflect fish back into the model domain. Reflective boundary was used outside of the event-based algorithm and was applied after all of the other algorithms for fish movement were applied and the individual was placed in its new location. The reflective boundary algorithm would be triggered when a fish was determined to have moved outside of the model domain. The fish was moved back to its position at the start of the time step, and then the surrounding cells were searched and the fish moved to the cell with the fewest boundaries. The angle was calculated as:

$$\theta(t) = \text{atan2}(yl(t) - y(t), xl(t) - x(t)) + 0.15 \cdot 2\pi \cdot (2 \cdot ran - 1) \tag{13}$$

where the values are the same as Eq. (5). The only change in the calculation of θ as compared to NS was the order of coordinate values in the atan2 function. Speed was calculated using the default swim speed (ss_0).

2.3 Algorithm selection

The event based algorithm chooses the movement algorithm that has the highest utility for each time step. Utilities are used to represent the costs and benefits that a particular behavior has on an animal's fitness (Anderson, 2002). For our purposes of avoidance of low DO, we only considered that avoiding hypoxia was critical to fitness. In evaluating the different algorithms, we did not factor in the costs of avoiding hypoxia or how decisions would affect growth, mortality, or reproduction. We computed three utility values for each time step based on the probabilities of two events indicative of immediate (e1) and prolonged (e2) exposure occurring:

$$U_{NS}(t) = util_{NS} \cdot prob_{NS}(t) \tag{14}$$

$$U_{sprint}(t) = util_{sprint} \cdot prob_{sprint}(t) \tag{15}$$

$$U_{CRW}(t) = util_{CRW} \cdot prob_{CRW}(t) \tag{16}$$

where util$_i$ is the intrinsic utility, and prob$_i$ is the probability of a triggered event. The intrinsic utility is the weight each
210 algorithm has in the utility calculation. Tactical algorithms have a higher weight than default or strategic algorithms and thus
are preferentially chosen. The probability of an event being triggered was calculated for NS and CCRW using the event of
immediate exposure (e1):

$$prob_{NS}(t) = (1.0 - mem_{NS}) \cdot e1(t) + mem_{NS} \cdot prob_{NS}(t - \Delta t) \tag{17}$$

215 $$prob_{CRW}(t) = (1.0 - mem_{CRW}) \cdot e1(t) + mem_{CRW} \cdot prob_{CRW}(t - \Delta t) \tag{18}$$

The probability for Sprint used event two (e2):

$$prob_{sprint}(t) = (1.0 - mem_{sprint}) \cdot e2(t) + mem_{sprint} \cdot prob_{sprint}(t - \Delta t) \tag{19}$$

The three probabilities are running averages of present and recent past hypoxia exposures and allow for the fish to have some
memory of past events. The utilities on each time step were then compared and the algorithm with the largest utility value
220 that exceeded a minimum threshold was selected. If none of the calculated utilities were larger than the threshold (hypoxia
exposure was not imminent and had not occurred in the recent past), then the default behavior was used. Parameters for Eqs.
(14) to (19) are given in Table 2.

2.4   Selection of static DO snapshots

Eight static DO snapshots were selected from the 240 hourly snapshots simulated during the 10 day (20–30 August 2002)
225 FVCOM-WASP simulation (Table 1). For each snapshot, a 2-D map and a 3-D map of DO were created. The snapshots
were selected based on a combination of the total area of sublethal DO and the degree of spatial variability in DO on each
of the 240 2-D maps. Area based on the full range of sublethal concentrations (DO of 2–4 mg L^{-1}), and for reference and
comparison also the hypoxic area (DO < 2 mg L^{-1}), were computed for each hourly time step. Also for each of the 240 time
steps, Ripley's K function (Kest in R), with isotropic edge correction, was computed that resulted in a plot of the statistic K
230 versus r (neighborhood in meters). The Ripley's K statistic measures the number of sublethal cells within the distance r so that K
generally increases with r. If the average number of sublethal cells within the neighborhood defined by distance r is greater than
the overall average sublethal cells throughout the map, then sublethal DO concentrations are considered to show clustering. A
common reference comparison is to the theoretical line defined by all sublethal cells being homogeneously distributed on the
map. To obtain a single value as an indicator of spatial variability so we could easily compare spatial variability across the 240
235 maps, we used the area under the curve (AUC) relating Ripley's K to r for each time step. When viewed across a wide range of
neighborhood sizes, larger AUC values imply greater spatial variability in sublethal DO concentrations.

To select the eight snapshots, we plotted AUC versus sublethal area and identified eight snapshots with moderate and high
sublethal areas that corresponded to the minimum, mean, and maximum AUC values (Table 1). For moderate sublethal areas we
selected two snapshots with minimum AUC and two snapshots with mean AUC; the maximum AUC was similar to the mean

240 so no maximum was selected. For the high sublethal area case, two snapshots were matched with minimum AUC and single snapshots with mean and maximum AUC values (Fig. 2). The duplicate snapshots for a given AUC provide information on the variability of simulation results when two different maps have similar sublethal areas and AUC values. Figure 3 illustrates the spatial variability in DO using maps of sublethal DO for one of the minimum AUC (Min-2) snapshots for the moderate sublethal area and another for the maximum AUC (Max) with the high sublethal area. The larger area of sublethal concentrations is seen

245 by the larger area of gray in the bottom versus top panels. When we visually compared maps of low versus high AUC for the same sublethal area (high or moderate), differences in the degree of clustering of sublethal areas between low and high AUC values were not obvious.

2.5   Design of simulations

Movement, and associated exposure to DO, was simulated using 913 individual fish for 10 days on each of the eight static maps

250 and the dynamic version. Simulations were done for the 2-D and 3-D maps and for good and poor avoidance competency. Good avoidance used the NS as described, while poor avoidance competency was achieved by changing the 0.15 value in Eq. (5) to 0.5, resulting in a much wider randomly-generated direction of movement during avoidance. Fish positions were updated every 15 minutes and DO in the dynamic maps changed every hour. Fish were initially placed in locations with favorable temperatures (about 26 °C) so that their initial spatial distribution was realistic for normoxic conditions (LaBone et al., 2017).

255 We present the results for the 2-D set of maps; similar patterns of spatial variability of effects on exposure were obtained for the 3-D set of maps (Supplemental Material). Movement parameters were set to values typical for croaker and related species (Table 2). Croaker is an abundant demersal-oriented fish in coastal waters of the northern GOM, especially in coastal waters off of Louisiana where hypoxia occurs annually. Extensive laboratory and field data available for DO effects on croaker have been previously used to specify realistic values for movement-related parameters (Rose et al., 2018b, a; LaBone et al., 2017,

260 2019).

Model outputs of fish locations and DO experienced every 15 minutes were analyzed to determine how spatial variability in DO affected exposure to hypoxia and sublethal DO concentrations. To illustrate the movement behavior, we show the detailed movement calculations (e1, e2, and the three probabilities and utilities) for a single fish for poor competency on a single static map (Min-2 of moderate sublethal area), and the movement tracks and DO experienced of four individual fish for good and

265 poor avoidance on two of the static DO snapshots. The DO experienced was color coded to show which movement algorithm was being used over time.

Exposure of all individuals was summarized over the 10 days for each fish by their cumulative exposure, which was calculated as the sum of the number of 15 minute time steps (expressed as days) each fish was exposed to DO less than 2 mg L^{-1}. Cumulative exposure to sublethal conditions was calculated the same as the exposure to hypoxia, except the overall sublethal

270 range of 2–4 mg L^{-1} (sublethal) was subdivided into 2–3 mg L^{-1} and 3–4 mg L^{-1} and each of these was considered the "exposed." We show plots of the cumulative exposure of all individual fish and also boxplots that summarize cumulative exposures over all fish. Outlier values were displayed in the box plots as points beyond the whiskers of the plot and were identified as values outside 1.5·IQR (interquartile range). The outliers are considered extreme but usable values, as they were not question-

able or suspicious "outlier" values in the statistical sense, and were therefore included in all analysis of model outputs. Another

275 summary of the exposure output was the percentage of fish on each time step between 2–3 mg L^{-1}. We focus on the 2–3 mg L^{-1} range for the sublethal analysis in this paper because it would have the most ecological effects on individuals (just above lethality) and the results for 3–4 mg L^{-1} were consistent with 2–3 mg L^{-1} but showed less overall variation and so the patterns were less clear. R was used for all statistical analysis and graphs (R Core Team, 2019).

3 Results

280 ### 3.1 Hypoxia avoidance in 2-D

Fish movement was a mix of the different behaviors, depending on the DO conditions they encountered (Figs. 4 and 5). Our example fish (Fig. 4) was immediately exposed to hypoxia that triggered the NS tactical avoidance (via e1) and also showed a slower rising utility for the CRW (strategic) as the fish's past exposure was considered. When the fish was unable to avoid waters with DO < 2 mg L^{-1} for 2 days (time step = 192, Fig. 4a), Sprint got invoked (Fig. 4b, c). Once the fish entered waters

285 with DO > 2 mg L^{-1} using Sprint, the utilities for both NS and CRW avoidance movement quickly returned to zero as exposures to DO > 2 mg L^{-1} accumulated (Fig. 4e). The fish then used default (CCRW) while moving among cells with DO > 2 mg L^{-1} (Fig. 4c). At time step 400, the fish wandered into water with DO < 2 mg L^{-1} causing the utilities for NS and CRW to rise (Fig. 4e) and triggering NS for an extended time period (time steps 475 to 600, Fig. 4c) as the fish moved around trying unsuccessfully to avoid waters with DO < 2 mg L^{-1}. Once NS enabled the fish to move to waters with DO > 2 mg L^{-1}, CRW

290 would briefly get triggered because of its history of exposure (Fig. 4c). Several more times the pattern of NS and CRW (both avoidance) were triggered (Fig. 4c, e), mostly keeping the fish in waters with DO > 2 mg L^{-1}, except for a few brief time periods (Fig. 4a). While the fish generally avoided hypoxia after the initial exposure and during the one extended period of hypoxia exposure (time steps 475 to 600), the fish was then always exposed to sublethal levels (2–4 mg L^{-1}) throughout the 10 days.

DO experienced and fish trajectories (Figs. 5 and 6) illustrated how a fish with good avoidance used NS (mostly straight

295 path) to escape the hypoxic zone, while several of the fish with poor avoidance had to use Sprint (perfectly straight path) after spending 48 hours in hypoxic conditions. Several of the selected fish used a mix of all four algorithms (all fish in Min-2 with poor competency), while other individuals used two or fewer algorithms that were dominated by default movement. The exposure patterns and variability in DO experienced also varied among individuals, even though these were maps with fixed spatial distributions of low DO. For example, individual #12 (Fig. 5b), after escaping hypoxia exposure, was exposed to DO

300 just above 2 mg L^{-1} throughout, while other individuals on certain maps (e.g., 425 on Min-2 with good competence, Fig. 5i) eventually went to waters with DO > 4 mg L^{-1}.

3.2 Hypoxia exposure

Cumulative exposure of individuals to hypoxia was higher under the high sublethal area snapshots compared to the moderate sublethal snapshots, with good competence showing the greater difference between moderate and high. With good avoidance

305 competency, most all fish showed exposures of about 1–2 days for maps with high sublethal area (Fig. 7a), which were further reduced to almost no exposure to hypoxia for moderate sublethal area maps (Fig. 8a). Sublethal area was positively correlated with hypoxic area (Table 1). Poor avoidance resulted in much more similar exposures between high and moderate sublethal conditions (Figs. 7b and 8b), which reflected that the fish have more randomness to their avoidance movement that masks some of the differences between the moderate and high sublethal area maps. Because of the effects of Sprint being triggered after

310 the first 48 hours for some fish under poor competency, we also examined the results using days 3 through 10 (Supplemental Material). The patterns in the results described for hypoxia exposure were less pronounced for the good competency results because there was little exposure to hypoxia after the first 48 hours when fish moved out of hypoxia and were effective at avoiding further exposure. However, removing the effects of the initial triggering of Sprint for poor competency simulations only slightly lowered overall hypoxic exposure, as fish continued to be exposed to hypoxia intermittently but with similar

315 percentage of individuals throughout the 10 days.

The effects of different degrees of spatial variability on hypoxia exposure were small. There was a weak suggestion that exposure to hypoxia decreased with increasing variability with the high sublethal area maps but increased with increasing variability for moderate sublethal area maps. This is seen by the tendency for exposure to decrease from left to right in each panel of Fig. 7, while exposure tended to increase from left to right in each panel of Fig. 8. This pattern of opposite effects of

320 spatial variability on hypoxia exposure being dependent on the degree of sublethal area, which is weak here, will become more apparent when sublethal exposure is examined.

3.3 Sublethal exposure

The effects of spatial variability on cumulative sublethal exposure to 2–3 mg L^{-1} of individuals showed higher exposure for high sublethal area (as expected – simply more possibility of exposure) and a tendency for opposite effects of variability between

325 high and moderate sublethal areas. For poor avoidance and especially for good avoidance competency, there was a subtle but consistent shifting to lower exposures with increasing variability for high sublethal area (points shifting to lower values from top to bottom in Fig. 9), while there was a shifting to higher exposures for the moderate sublethal area maps (less open space near top of each plot, except for dynamic, in Fig. 10).

This opposite effect of variability was more apparent when the exposures of fish to 2–3 mg L^{-1} was examined as the percent

330 of all individuals. Under high sublethal area, the percent of fish exposed to 2–3 mg L^{-1} decreased with increasing variability for both good competency (Fig. 11a) and poor competency (Fig. 11b). The green lines (min AUC, low variability) had the highest exposure, while the purple lines (max) and magenta lines (dynamic map) had the lowest exposures. For good competency, averaged percent of individuals exposed to 2–3 mg L^{-1} over the 10 days was 46% and 47% for the two min variability maps, 39% for the mean map, and 37% for the max map. A similar range (maximum minus minimum) of averaged percent exposed

335 of about 8% occurred with poor competency: 37% and 38% for min variability, 32% for mean, and 30% for the max map. In both cases, the percent exposure for the dynamic maps were within the values of their respective static maps (38% for the good competency and 29% for poor competency).

The opposite pattern was predicted for the moderate sublethal area conditions (Fig. 12); percent exposed to 2–3 mg L^{-1} increased, rather than decreased, with increasing variability. In Fig. 12, the green lines (2 min AUC maps) showed the lowest

340 exposures while the orange line (mean AUC) and magenta line (dynamic) showed the highest exposures. For good competency, averaged percent of individuals exposed to 2–3 mg L^{-1} was 36% for the two min variability maps and 40% and 43% for the mean maps, also a range of about 8%. For poor competency, there was little difference in percent exposed from min and mean maps: 28% for the two min maps and 29% for the two mean maps. This lack of a difference was also due to the inclusion of the first two days when exposure was similarly low on all of the maps due to Sprint, but the differences after day 2 were still

345 not strong.

The opposite effects of spatial variability between moderate and high sublethal areas were maintained for 3-D simulations and the effects were maintained, but smaller, for exposure to 3–4 mg L^{-1}. The exposure patterns for exposure to 2–3 mg L^{-1} were maintained after the first 48 hours of exposures so that Sprint was not overly influential on the patterns and also under 3-D conditions demonstrating the results were robust to including an option for vertical avoidance (Supplemental Material). For

350 both moderate and high sublethal areas, the opposite effects of spatial variability were similar but less apparent for exposure to 3–4 mg L^{-1} because exposures in general showed less variation among simulations for 3–4 mg L^{-1} (results not shown).

4   Discussion

The spatial variability of DO in the Gulf of Mexico, and likely in other places with chronic river-driven seasonal hypoxia, is patchier than we envisioned. As measurements become more resolved and hydrodynamic-water quality models more detailed,

355 what was once considered a continuous area of hypoxia now reveals itself to have a much more spatial structure. The persistence at a location, the dissipation and reforming of hypoxia in response to weather events, local bathymetric influences (e.g., Virtanen et al., 2019), and other factors, all contribute to the spatial variability in the hypoxic and sublethal DO concentrations (Bianchi et al., 2010; Rabalais and Turner, 2019). The rather smooth looking earlier annual spatial maps obtained from monitoring data (e.g., Rabalais et al., 2001) are continually evolving into more irregular shapes with highly dynamic boundaries and patchiness

360 (Zhang et al., 2009; Obenour et al., 2013; Justić and Wang, 2014). Further, while we focus on the hypoxic waters, most mobile organisms show avoidance behavior making the dynamics of sublethal concentrations (often not avoided) highly relevant ecologically. Hypoxia causes mortality, which is a major consideration at the population level, but the population effects also depend on the fraction of the population that is exposed. Reduced growth, lowered fecundity, and indirect effects from displacement may have a less obvious influence on the population than mortality but if a much larger percent of the population

365 are exposed, these sublethal effects can lead to ecologically-significant population-level responses that, in some cases, can exceed the effects from direct mortality (Rose et al., 2009). Fish movement, spatial variability in DO, and exposure to lethal and sublethal concentrations are complicated. However, knowing exposure is critical in order to make accurate predictions of the effects of low DO on individuals, which then can be scaled to the responses of populations and food webs (Rose et al., 2009, 2018b, a; De Mutsert et al., 2016). In this paper, we are using simulation methods to explore this issue of how spatial

370 variability in DO would affect exposure of fish to hypoxia and sublethal concentrations of DO.

Our a priori intuitive thinking was that more spatially-variable DO would lead to higher exposure to hypoxia. A fixed stable hypoxic area would allow most fish to avoid the area and minimize exposure once they have adjusted to the initial encounter. Patchy or clustered locations of hypoxia would mean that fish would have to continually deal with possible exposure and there would be many more opportunities for swimming into low DO water. We also assumed that because waters with sublethal DO levels would be associated (loosely adjacent) with hypoxia, more avoidance of hypoxia would also result in higher exposure to sublethal DO. If the patchiness was also dynamic in time, then that would seem to further increase the chances of encountering low DO water and thereby increase exposure even more. Our analysis reveals important details, nuances, and incorrect aspects of this intuitive (conceptual-level) view of how spatial variability in DO would affect fish exposure.

Our refined view of how spatial variability affects exposure distinguishes between hypoxia and sublethal exposures and shows that effects of spatial variability on sublethal exposure can reverse depending on the areal extent of low DO waters. Model simulations showed that exposure to hypoxia was, as expected, greatly influenced by the swimming avoidance competency assumed for the fish. Given other conditions were the same, good competency (little randomness to avoidance response) resulted in less exposure to hypoxia than poor competency (left (a) versus right (b) panels in Figs. 7 and 8). Further, good competency essentially eliminated exposure to hypoxic conditions. Most all exposure to hypoxia occurred in the first 24 to 48 hours, and this was generally low (Fig. 7a). Beyond the initial exposures (i.e., using days 3–10), good competency resulted in near-zero exposure to hypoxia (Supplemental Material). In contrast, exposure to hypoxia with poor competency showed persistent and relatively higher exposure to hypoxia that occurred throughout the ten days of the simulations (results not shown). Such persistent exposure occurred even when the effects of initial use of Sprint in the first 48 hours were eliminated (Supplemental Material).

Despite the differences in exposure to hypoxia with good versus poor competency, both resulted in relatively high exposures to sublethal DO concentrations. Roughly, 30 to 50% of the individuals were exposed to 2–3 mg L^{-1} and this occurred, except for the 48 hours that triggered Sprint, throughout the 10 days of most all of the simulations (Figs. 11 and 12). Interestingly, the percent of individuals exposed to 2–3 mg L^{-1} was often somewhat higher (about 5–10%) for good competency compared to poor competency. The reason is that good competency resulted in fewer individuals being exposed to hypoxia and so more individuals were available to be exposed to sublethal concentrations. If an individual was successful at avoiding hypoxia, they likely were then exposed to sublethal concentrations. Our results do not support the idea that fish with good avoidance behavior ameliorate the ecological effects of low DO. Rather, even fish with good avoidance abilities are exposed to sublethal concentrations and good avoidance may shift individuals from lethal to sublethal exposures rather than to no-effects. Our results also showed that this occurred when the fish were given the option to swim vertically to avoid hypoxia (Supplemental Material). We need to accurately predict avoidance behavior in order to quantify the effects of hypoxia exposure on mortality and the effects of exposure to sublethal concentrations on growth and reproduction.

The effects of spatial variability in DO on sublethal exposure were opposite depending on the degree of sublethal area. Exposure to 2–3 mg L^{-1} decreased with increasing variability for maps with high sublethal area but increased with variability for maps with moderate sublethal area (reverse ordering of line colors between Figs. 11 and 12). One possibility is that our measure of spatial variability (Ripley's K, Fig. 2) did not capture variability but rather reflected some other feature of the

DO concentrations (e.g., co-occurrence of sublethal with lethal areas) related to high versus moderate sublethal areas. Spatial maps of DO for different degrees of spatial variability did not show obvious and dramatic differences in the spatial patterns of sublethal DO concentrations (Fig. 3). Furthermore, we used an aggregate measure (area under the curve) to further summarize the Ripley's K values, which generates a series of values for increasing spatial neighborhoods (K versus r in Fig. 2). With our

410 maps showing Ripley's K values above the theoretical value for our maps implies the "patches" of sublethal DO concentrations are all more clustered than randomly distributed. If our summarization of Ripley's K values is valid, then higher AUC values suggest that the patches of sublethal concentrations are more clustered over a range of spatial scales. The similarity of exposures for "replicate" maps (i.e., similar AUC values) show that our patterns of exposure with variability are robust. If the AUC values reflect overall spatial variability, then our results clearly demonstrate that quantifying exposure is a complicated overlaying of

415 spatial DO with moving fish that depends on relatively subtle differences in the amount of low DO area, its spatial distribution, and the avoidance abilities assumed for the fish movement behavior.

We hypothesize that spatial variability in DO has opposite effects on exposure depending on the degree of sublethal area due to effects of how individuals encounter the patches of sublethal concentrations as a result of avoidance of hypoxia. With high sublethal area there is also high hypoxic area (Table 1) and thus individuals frequently used avoidance. These active individuals

420 avoid hypoxia but with higher clustering of sublethal areas there are locations (refuge areas adjacent to hypoxic areas) to move to that are normoxic (i.e., not sublethal). With relatively low Ripley's K (lower spatial variability), the patches of sublethal concentrations are more evenly distributed and thus fish avoiding hypoxia are more likely to encounter a sublethal patch.

The opposite pattern for moderate sublethal area is also about encounters. Rather than clustering creating refuges when there is high degree of sublethal area, clustering with moderate sublethal area creates more opportunities for individuals to

425 encounter the relatively rare sublethal concentrations. With relatively low Ripley's K values, the same moderate sublethal area consists of dispersed patches. This creates many opportunities for individuals that avoid hypoxia to locate in high DO cells. We might expect that higher spatial variability in the case of moderate sublethal area results in a subset of individuals inhabit areas with hypoxia associated with sublethal concentrations and thus some individuals should show persistent exposure to sublethal concentrations. Our hypothesis is speculative and should be investigated further using designed simulation experiments and by

430 following the DO experienced over time across many individuals. Additional statistical analysis of the spatial heterogeneity in sublethal areas beyond Ripley's K is also needed to better understand the spatial features that drive the changes in exposure between high and moderate sublethal area maps.

We initially considered that the dynamic map would generate exposure results acting as the most spatially variable map. Not only were there differences among cells in the dynamic maps, but also the DO in each cell changed every hour. Sublethal

435 exposure with the dynamic maps did, as expected, have the lowest exposure for the high sublethal area (magenta lines in Fig. 11) that continued the trend of decreasing exposure with increasing variability. However, the sublethal exposure for the dynamic maps with the moderate sublethal area was inconclusive (Fig. 12). The line for the dynamic map crossed several times with the lines for min and mean AUC maps in both the good and poor competency simulations. When viewed more generally, the sublethal exposures with the dynamic maps were all generally within the range of exposures predicted over the static maps

440 confirming that our results for static maps also apply to the more realistic situation of temporally and spatially varying DO

maps. Our results are not sufficient to determine how temporally dynamic DO combines with the spatial variability in DO to affect sublethal exposures. However, it is encouraging that our results suggest that knowing about spatial variability of low DO concentrations can enable realistic estimation of exposure even under temporally-dynamic conditions. Additional simulations that use DO seascapes with known combinations of spatial and temporal variation are needed to further untangle the effects of
445   spatial and temporal variation in DO on exposure.

Another result from our analysis that complicates quantifying exposure to hypoxia and sublethal DO concentrations is the very high level of variability in exposure predicted among individuals (Figs. 9 and 10). Given simulations were for 10 days with individuals released within a region of the hypoxic zone and with static DO maps, one might expect exposure (either low or high) would be similar among individuals. Yet, even under these conditions of exposure with an assumed competency and
450   static DO conditions, inter-individual variation in exposure was substantial. The effects of constant and time-varying exposures on growth and fecundity can be non-linear (e.g., threshold or accelerating effects) at the level of individual (McNatt and Rice, 2004; Neilan and Rose, 2014) and hypoxia effects can be interactive with other factors and stressors (McBryan et al., 2013; Breitburg et al., 2019). Thus, using an exposure averaged over individuals (and/or averaged over time such as weekly) to assess ecological responses will likely underestimate effects that occur with exposures to low DO. Coiro et al. (2000) showed that the
455   growth reduction in grass shrimp with fluctuating exposures was less than if the minimum DO of the cycle was used but had larger effects than if the time-averaged DO concentration was used.

Using our simulation results, we can illustrate the potential for spatial averaging to generate inaccurate predictions of exposure that lead to underestimation of sublethal effects. We selected the exposure of the 913 individuals for the 24 hours of day 5 for one of the 10-day simulations (high sublethal area, good competency, Fig. 11a) to illustrate the effects of averaging. We
460   can link exposure to the sublethal effect of reduced growth by using the equation from Neilan and Rose (2014):

$$f = 1.0 - 110.78 \frac{(3.35 - DO_t)^2}{(3.35 - DO_t)^2 + 21.06^2} \tag{20}$$

where DO_t is the exposure DO concentration of an individual at time t. This equation is used for DO concentrations less than 3.35 mg L^{-1}, above which f equals 1. The equation was estimated using laboratory experiments on low DO effects on growth and generates the reduction from normoxic growth from the DO concentration experienced by an individual. We used this
465   equation in earlier simulations of hypoxia effects on croaker (Rose et al., 2018b, a). Using the first 15 minute timestep of hour 1 of day 5 only, we grouped fish into increasingly larger cells (and used averaged DO and f values for each cell) to mimic the spatial resolution typical of population and food web models. High resolution (100 m to 1 km cells) show similar exposure DO concentrations and f values (mean, median, percentiles) as compared to using each fish as an individual value because the DO maps showed spatial correlation on the km-scale and nearby fish had similar exposures. At 10 km by 10 km resolution, we
470   obtained 285 values with cells having between zero and 10 individuals. The 25th percentile exposure DO was 2.64 versus 2.54 mg L^{-1} and the 5th percentile was 2.11 versus 2.05 mg L^{-1}. The 25th percentile for the f value was 0.88 versus 0.84 and the 5th was 0.62 versus 0.58. This effect increases as we used coarser resolutions. For example, for 50 km resolution (31 cells with fish), the 5th percentile of the f values becomes 0.8 versus 0.58 for all fish treated separately. Another way to summarize the underestimation is the percent of fish (each individual or individuals averaged by cell) below an f value of 0.75: 18% for all

475   individuals, 16% for 10 km cells, and 3% for 50 km cells. Similar mis-estimation can occur with temporal averaging. Models that attempt to scale hypoxic and sublethal DO effects to higher levels such as the population must carefully consider the effects of aggregation (e.g., modeling total biomass rather than individuals), the spatial scales of variation in the DO map, and the effects of temporal and spatial averaging of DO within cells that then determine exposure.

    Our ability to measure movement trajectories and patterns, including the DO experienced by individuals, is rapidly increas-
480   ing (Svendsen et al., 2006; Hussey et al., 2015; Hays et al., 2016). Field methods are allowing for detailed resolution of fish movement behavior in response to DO (e.g., Brady and Targett, 2013) and chemical methods (e.g., stable isotopes, Limburg et al., 2015; Mohan and Walther, 2016) are becoming available for determining recent exposure to hypoxia. Relatively soon, we will be able to challenge the assumptions and skill of fish movement models and avoidance behaviors like that implemented in this analysis with correspondingly resolved field data. Subsequent analyses will use our results about fine-scale exposure
485   to refine movement and avoidance algorithms. In addition to algorithms that also match the trajectories of individuals, bioenergetics of movement (such as costs of avoidance) can be included. Such information will enable refinement of our earlier 2-D population dynamics modeling of hypoxia effects (Rose et al., 2018b, a) and hopefully inform other population and food web modeling. By following hundreds of thousands of individuals within 3-D hydrodynamic-water quality models, we aim to predict fish population-level responses to hypoxia under management actions designed to control nutrient inputs.

490   **5   Conclusions**

We used 2-D and 3-D simulations of individual fish movement within a FVCOM-WASP coupled hydrodynamics-water quality model to show how spatial variability in DO affects exposure of fish to hypoxia and to sublethal DO concentrations. Our results showed that accurate estimation of exposure depends on both the degree of clumpiness of sublethal DO concentrations and the total area of sublethal DO. Exposure to sublethal concentrations occurred under all conditions examined regardless of the fish's
495   ability to avoid hypoxia, including good and poor competency of fish for avoidance, and allowing for vertical avoidance movement (3-D). Accurate estimation of exposure, especially to sublethal DO concentrations, is critical for assessing how increasing or reducing hypoxic zones in coastal waters will affect ecological effects of low DO (e.g., reduced growth) on fish. Simulating individual fish within high-resolution 3-D coupled hydrodynamic-biogeochemical models enables the movement behavior of fish to be combined with spatially and temporally varying DO concentrations to obtain realistic estimation of exposures. As the
500   measurement methods for documenting fish movement trajectories and estimation of DO exposure of fish in the field continue to be refined, we will very soon be able to rigorously challenge the realism and skill of coupled biophysical models such as used here with empirical data. Isolated testing of fish movement using short-term static DO maps is necessary for understanding how the movement algorithms operate and provides the basis for then using these algorithms in more complicated population dynamics and food web models that simulate dynamic environmental and biological conditions.

Author contributions. EL, KR, and DJ designed the experiments and prepared the paper. HH contributed to model development. LW provided FVCOM-WASP model output. EL performed experiments, analyzed data, and visualized data.

Competing interests. The authors declare that they have no conflict of interest.

Acknowledgements. E.D. LaBone was supported by the NSF Graduate Research Fellowships Program and the Louisiana Board of Regents 8g Fellowship. The project was funded in part by the NOAA/CSCOR Northern Gulf of Mexico Ecosystems and Hypoxia Assessment Program under awards NA09NOS4780230 and NA16NOS4780204 to Louisiana State University. Portions of this research were conducted with high performance computing resources provided by Louisiana State University (http://www.hpc.lsu.edu). We would also like to thank Thomas LaBone for advice on statistics.

References

Anderson, J. J.: An Agent-based Event Driven Foraging Model, Natural Resource Modeling, 15, 55–82, 2002.

515   Babin, B.: Factors affecting short-term oxygen variability in the northern Gulf of Mexico hypoxic zone, Phd dissertation, Louisiana State University, Baton Rouge, 2012.

Babin, B. L. and Rabalais, N. N.: Trends in oxygen variability in the northern Gulf of Mexico hypoxic zone, in: OCEANS 2009, pp. 1–4, https://doi.org/10.23919/OCEANS.2009.5422223, 2009.

Baustian, M. M., Craig, J. K., and Rabalais, N. N.: Effects of summer 2003 hypoxia on macrobenthos and Atlantic croaker foraging selectivity

520   in the northern Gulf of Mexico, Journal of Experimental Marine Biology and Ecology, 381, S31–S37, 2009.

Bell, G. and Eggleston, D.: Species-specific avoidance responses by blue crabs and fish to chronic and episodic hypoxia, Marine Biology, 146, 761–770, 2005.

Bianchi, T., DiMarco, S., Cowan Jr, J., Hetland, R., Chapman, P., Day, J., and Allison, M.: The science of hypoxia in the Northern Gulf of Mexico: a review, Science of the Total Environment, 408, 1471–1485, 2010.

525   Booth, J., Woodson, C., Sutula, M., Micheli, F., Weisberg, S., Bograd, S., Steele, A., Schoen, J., and Crowder, L.: Patterns and potential drivers of declining oxygen content along the southern California coast, Limnology and Oceanography, 59, 1127–1138, 2014.

Brady, D. C. and Targett, T. E.: Movement of juvenile weakfish Cynoscion regalis and spot Leiostomus xanthurus in relation to diel-cycling hypoxia in an estuarine tidal tributary, Marine Ecology Progress Series, 491, 199–219, 2013.

Breitburg, D., Hondorp, D., Davias, L., and Diaz., R.: Hypoxia, nitrogen, and fisheries: integrating effects across local and global landscapes,

530   Annual Review of Marine Science, 1, 329–349, 2009.

Breitburg, D., Levin, L. A., Oschlies, A., Grégoire, M., Chavez, F. P., Conley, D. J., Garçon, V., Gilbert, D., Gutiérrez, D., Isensee, K., Jacinto, G. S., Limburg, K. E., Montes, I., Naqvi, S. W. A., Pitcher, G. C., Rabalais, N. N., Roman, M. R., Rose, K. A., Seibel, B. A., Telszewski, M., Yasuhara, M., and Zhang, J.: Declining oxygen in the global ocean and coastal waters, Science, 359, https://doi.org/10.1126/science.aam7240, 2018.

535   Breitburg, D., Baumann, H., Sokolova, I., and Frieder, C.: Multiple stressors – forces that combine to worsen deoxygenation and its effects, in: Ocean deoxygenation: Everyone's problem - Causes, impacts, consequences and solutions, edited by Laffoley, D. and Baxter, J., pp. xxii+562pp, IUCN, Gland, Switzerland, 2019.

Chen, C., Beardsley, R., Cowles, G., Qi, J., Lai, Z., Gao, G., Stuebe, D., Xu, Q., Xue, P., Ge, J., Ji, R., Hu, S., Tian, R., Huang, H., Wu, L., and Lin., H.: An Unstructured Grid, Finite-Volume Coastal Ocean Model: FVCOM User Manual, Third Edition, Tech. Rep.

540   SMAST/UMASSD-11-1101, Sea Grant College Program, Massachusetts Institute of Technology, Cambridge, MA, 2011.

Coiro, L., Poucher, S., and Miller, D.: Hypoxic effects on growth of Palaemonetes vulgaris larvae and other species: Using constant exposure data to estimate cyclic exposure response, Journal of Experimental Marine Biology and Ecology, 247, 243–255, 2000.

Craig, J. K.: Aggregation on the edge: effects of hypoxia avoidance on the spatial distribution of brown shrimp and demersal fishes in the Northern Gulf of Mexico, Marine Ecology Progress Series, 445, 75–95, http://www.int-res.com/abstracts/meps/v445/p75-95/, 2012.

545   De Mutsert, K., Steenbeek, J., Lewis, K., Buszowski, J., Cowan Jr, J., and Christensen, V.: Exploring effects of hypoxia on fish and fisheries in the northern Gulf of Mexico using a dynamic spatially explicit ecosystem model, Ecological Modelling, 331, 142–150, 2016.

Del Giudice, D., Matli, V., and Obenour, D.: Bayesian mechanistic modeling characterizes Gulf of Mexico hypoxia: 1968–2016 and future scenarios, Ecological Applications, https://doi.org/doi.org/10.1002/eap.2032, 2019.

DiMarco, S. F., Chapman, P., Walker, N., and Hetland, R. D.: Does local topography control hypoxia on the eastern Texas–Louisiana shelf?, Journal of Marine Systems, 80, 25–35, 2010.

Eby, L. A. and Crowder, L. B.: Hypoxia-based habitat compression in the Neuse River Estuary: context-dependent shifts in behavioral avoidance thresholds, Canadian Journal of Fisheries and Aquatic Sciences, 59, 952–965, 2002.

Fennel, K., Hu, J., Laurent, A., Marta-Almeida, M., and Hetland, R.: Sensitivity of hypoxia predictions for the northern Gulf of Mexico to sediment oxygen consumption and model nesting, Journal of Geophysical Research: Oceans, 118, 990–1002, https://doi.org/10.1002/jgrc.20077, 2013.

Fennel, K., Laurent, A., Hetland, R., Justić, D., Ko, D., Lehrter, J., Murrell, M., Wang, L., Yu, L., and Zhang, W.: Effects of model physics on hypoxia simulations for the northern Gulf of Mexico: A model intercomparison, Journal of Geophysical Research: Oceans, 121, 5731–5750, 2016.

Hays, G., Ferreira, L., Sequeira, A., Meekan, M., Duarte, C., Bailey, H., Bailleul, F., Bowen, W., Caley, M., Costa, D., and Eguíluz, V.: Key questions in marine megafauna movement ecology, Trends in Ecology and Evolution, 31, 463–475, 2016.

Hrycik, A. R., Almeida, L. Z., and Höök, T. O.: Sub-lethal effects on fish provide insight into a biologically-relevant threshold of hypoxia, Oikos, 126, 307–317, 2017.

Hussey, N., Kessel, S., Aarestrup, K., Cooke, S., Cowley, P., Fisk, A., Harcourt, R., Holland, K., Iverson, S., Kocik, J., and Flemming, J.: Aquatic animal telemetry: a panoramic window into the underwater world, Science, 348, p.1255 642, 2015.

Justić, D. and Wang, L.: Assessing temporal and spatial variability of hypoxia over the inner Louisiana–upper Texas shelf: Application of an unstructured-grid three-dimensional coupled hydrodynamic-water quality model, Continental Shelf Research, 72, 163–179, 2014.

Justic, D., Rabalais, N. N., and Turner, R. E.: Effects of climate change on hypoxia in coastal waters: A doubled CO_2 scenario for the northern Gulf of Mexico, Limnology and Oceanography, 41, 992–1003, 1996.

Justic, D., Rabalais, N. N., and Turner, R. E.: Simulated responses of the Gulf of Mexico hypoxia to variations in climate and anthropogenic nutrient loading, Journal of Marine Systems, 42, 115–126, 2003.

Kareiva, P. M. and Shigesada, N.: Analyzing insect movement as a correlated random walk, Oecologia, 56, 234–238, 1983.

LaBone, E., Justic, D., Rose, K., Wang, L., and Huang, H.: Modeling Fish Movement in 3-D in the Gulf of Mexico Hypoxic Zone, Estuaries and Coasts, 42, 1662–1685, https://doi.org/10.1007/s12237-019-00601-6, 2019.

LaBone, E. D., Justic, D., Rose, K., Wang, L., and Huang, H.: Comparing Default Movement Algorithms for Individual Fish Avoidance of Hypoxia in the Gulf of Mexico, in: Modeling Coastal Hypoxia: Numerical Simulations of Patterns, Controls and Effects of Dissolved Oxygen Dynamics, edited by Justic, D., Rose, K., Hetland, R., and Fennel, K., pp. 239–278, Springer International, New York City, 2017, 2017.

Lehrter, J., Ko, D., Lowe, L., and Penta, B.: Predicting effects of global climate change in Northern Gulf of Mexico hypoxia., in: Modeling coastal hypoxia: Numerical simulations of patterns, controls and effects of dissolved oxygen dynamics, edited by Justic, D., Rose, K., Hetland, R., and Fennel, K., pp. 173–214, Springer International, New York City, 2017.

Levin, L., Ekau, W., Gooday, A., Jorissen, F., Middelburg, J., Naqvi, S., Neira, C., Rabalais, N., and Zhang, J.: Effects of natural and human-induced hypoxia on coastal benthos, Biogeosciences, 6, 2063–2098, 2009.

Limburg, K., Walther, B., Lu, Z., Jackman, G., Mohan, J., Walther, Y., Nissling, A., Weber, P., and Schmitt, A.: In search of the dead zone: use of otoliths for tracking fish exposure to hypoxia, Journal of Marine Systems, 141, 167–178, 2015.

McBryan, T., Anttila, K., Healy, T. M., and Schulte., P. M.: Responses to temperature and hypoxia as interacting stressors in fish: Implications for adaptation to environmental change, Integrative and Comparative Biology, 53, 648–659, 2013.

McNatt, R. and Rice, J.: Hypoxia-induced growth rate reduction in two juvenile estuary-dependent fishes, Journal of Experimental Marine Biology and Ecology, 311, 147–156, 2004.

Mohan, J. and Walther, B.: Out of breath and hungry: natural tags reveal trophic resilience of Atlantic croaker to hypoxia exposure, Marine Ecology Progress Series, 560, 207–221, https://doi.org/https://doi.org/10.3354/meps11934, 2016.

Muller, A., Muller, D., and Muller, A.: Resolving spatiotemporal characteristics of the seasonal hypoxia cycle in shallow estuarine environments of the Severn River and South River, MD, Chesapeake Bay, USA, Heliyon, 2, e00 157, 2016.

Neilan, R. M. and Rose, K.: Simulating the effects of fluctuating dissolved oxygen on growth, reproduction, and survival of fish and shrimp, Journal of Theoretical Biology, 343, 54–68, https://doi.org/10.1016/j.jtbi.2013.11.004, 2014.

Obenour, D., Michalak, A., and Scavia, D.: Assessing biophysical controls on Gulf of Mexico hypoxia through probabilistic modeling, Ecological Applications, 25, 492–505, 2015.

Obenour, D. R., Scavia, D., Rabalais, N. N., Turner, R. E., and Michalak, A. M.: Retrospective analysis of midsummer hypoxic area and volume in the northern Gulf of Mexico, 1985–2011, Environmental science & technology, 47, 9808–9815, 2013.

Pollock, M., Clarke, L., and Dubé, M.: The effects of hypoxia on fishes: from ecological relevance to physiological effects, Environmental Reviews, 15, 1–14, 2007.

R Core Team: R: A Language and Environment for Statistical Computing, R Foundation for Statistical Computing, Vienna, Austria, https://www.R-project.org/, 2019.

Rabalais, N. and Turner, R.: Gulf of Mexico Hypoxia: Past, Present, and Future, Limnology and Oceanography Bulletin, 28, 117–124, 2019.

Rabalais, N. N., Turner, R. E., and Wiseman Jr, W. J.: Hypoxia in the Gulf of Mexico, J. Environ. Qual, 30, 320–329, 2001.

Rabalais, N. N., Turner, R. E., and Wiseman Jr, W. J.: Gulf of Mexico Hypoxia, aka" The Dead Zone", Annual Review of Ecology and Systematics, 33, 235–263, 2002.

Rabalais, N. N., Turner, R. E., Sen Gupta, B. K., Boesch, D. F., Chapman, P., and Murrell, M. C.: Hypoxia in the northern Gulf of Mexico: Does the science support the plan to reduce, mitigate, and control hypoxia?, Estuaries and Coasts, 30, 753–772, 2007.

Rabalais, N. N., Diaz, R. J., Levin, L. A., Turner, R. E., Gilbert, D., and Zhang, J.: Dynamics and distribution of natural and human-caused hypoxia, Biogeosciences, 7, 585–619, 2010.

Roman, M., Pierson, J., Kimmel, D., Boicourt, W., and Zhang, X.: Impacts of hypoxia on zooplankton spatial distributions in the northern Gulf of Mexico, Estuaries and Coasts, 35, 1261–1269, 2012.

Roman, M., Brandt, S., Houde, E., and Pierson, J.: Interactive Effects of Hypoxia and Temperature on Coastal Pelagic Zooplankton and Fish, Frontiers in Marine Science, 6, p.139, https://doi.org/0.3389/fmars.2019.00139, 2019.

Rose, K., Adamack, A., Murphy, C., Sable, S., Kolesar, S., Craig, J., Breitburg, D., Thomas, P., Brouwer, M., Cerco, C., and Diamond, S.: Does hypoxia have population-level effects on coastal fish? Musings from the virtual world, Journal of Experimental Marine Biology and Ecology, 381, S188–S203, 2009.

Rose, K., Justic, D., Fennel, K., and Hetland, R.: Numerical modeling of hypoxia and its effects: Synthesis and going forward, in: Modeling coastal hypoxia: Numerical simulations of patterns, controls and effects of dissolved oxygen dynamics, edited by Justic, D., Rose, K., Hetland, R., and Fennel, K., p. 401–421, Springer International, New York City, 2017.

Rose, K., Creekmore, S., Justić, D., Thomas, P., Craig, J., Neilan, R. M., Wang, L., Rahman, M. S., and Kidwell, D.: Modeling the population effects of hypoxia on Atlantic croaker (Micropogonias undulatus) in the northwestern Gulf of Mexico: part 2—realistic hypoxia and eutrophication, Estuaries and Coasts, 41, 255–279, 2018a.

Rose, K., Creekmore, S., Thomas, P., Craig, J., Rahman, M., and Neilan, R.: Modeling the population effects of hypoxia on Atlantic croaker

625   (Micropogonias undulatus) in the northwestern Gulf of Mexico: part 1—model description and idealized hypoxia, Estuaries and Coasts,

        41, 233–254, 2018b.

Rose, K. A., Huang, H., Justic, D., and de Mutsert, K.: Simulating Fish Movement Responses to and Potential Salinity Stress from Large-

        Scale River Diversions, Marine and Coastal Fisheries, 6, 43–61, https://doi.org/10.1080/19425120.2013.866999, 2014.

Sanford, L., Sellner, K., and Breitburg, D.: Covariability of dissolved oxygen with physical processes in the summertime Chesapeake Bay,

630   Journal of Marine Research, 48, 567–590, 1990.

Scavia, D., Bertani, I., Obenour, D., Turner, R., Forrest, D., and Katin, A.: Ensemble modeling informs hypoxia management in the northern

        Gulf of Mexico, Proceedings of the National Academy of Sciences, 114, 8823–8828, 2017.

Shimps, E., Rice, J., and Osborne, J.: Hypoxia tolerance in two juvenile estuary-dependent fishes, Journal of Experimental Marine Biology,

        325, 145–162, 2005.

635 Sperna Weiland, F. C., Van Beek, L. P. H., Kwadijk, J. C. J., and Bierkens, M. F. P.: Global patterns of change in discharge regimes for 2100,

        Hydrology and Earth System Sciences, 16, 1047–1062, 2012.

Stierhoff, K., Targett, T., and Miller, K.: Ecophysiological responses of juvenile summer and winter flounder to hypoxia: experimental and

        modeling analyses of effects on estuarine nursery quality, Marine Ecology Progress Series, 325, 255–266, 2006.

Svendsen, J., Aarestrup, K., Steffensen, J., and Herskin, J.: Novel acoustic dissolved oxygen transmitter for fish telemetry, Marine Technology

640   Society Journal, 40, 103–108, 2006.

Thomas, P. and Rahman, M.: Extensive reproductive disruption, ovarian masculinization and aromatase suppression in Atlantic croaker in

        the northern Gulf of Mexico hypoxic zone, Proceedings of the Royal Society of London B, 279, 28–38, 2012.

Turner, R. E. and Rabalais, N. N.: Changes in Mississippi River water quality this century, BioScience, 41, 140–147, 1991.

Vaquer-Sunyer, R. and Duarte, C.: Thresholds of hypoxia for marine biodiversity, Proceedings of the National Academy of Sciences, 105,

645   15 452–15 457, 2009.

Virtanen, E., Norkko, A., Nyström Sandman, A., and Viitasalo, M.: Identifying areas prone to coastal hypoxia–the role of topography,

        Biogeosciences, 16, 3183–3195, 2019.

Wang, L. and Justic, D.: A modeling study of the physical processes affecting the development of seasonal hypoxia over the inner Louisiana-

        Texas shelf: Circulation and stratification, Continental Shelf Research, 29, 1464–1476, 2009.

650 Watkins, K. S. and Rose, K. A.: Evaluating the performance of individual-based animal movement models in novel environments, Ecological

        Modelling, 250, 214–234, 2013.

Wool, T., Ambrose, R., Martin, J., and Comer, E.: Water quality analysis simulation program (WASP), User's Manual, Version 6, Environ-

        mental Protection Agency, Washington, DC, 2006.

Wu, H.-i., Li, B.-L., Springer, T. A., and Neill, W. H.: Modelling animal movement as a persistent random walk in two dimensions: expected

655   magnitude of net displacement, Ecological Modelling, 132, 115–124, 2000.

Zhang, H., Ludsin, S., Mason, D., Adamack, A., Brandt, S., Zhang, X., Kimmel, D., Roman, M., and Boicourt, W.: Hypoxia-driven changes

        in the behavior and spatial distribution of pelagic fish and mesozooplankton in the northern Gulf of Mexico, Journal of Experimental

        Marine Biology and Ecology, 38, S80–S91, 2009.

Zhang, H., Mason, D., Stow, C., Adamack, A., Brandt, S., Zhang, X., Kimmel, D., Roman, M., Boicourt, W., and Ludsin, S.: Effects of

660   hypoxia on habitat quality of pelagic planktivorous fishes in the northern Gulf of Mexico, Marine Ecology Progress Series, 505, 209–226,

        2014.

Table 1. Areas (hypoxic and sublethal, km^2 and percent of grid) and AUC (area under the curve) values for eight snapshots selected from the hourly DO maps generated by FVCOM-WASP simulation of 10 days (20-30 August 2002). Sublethal DO was defined as 2–4 mg L^{-1}. Based on the sublethal area and AUC values, each snapshot was labeled by category of total sublethal area (high or moderate) and by category of AUC (minimum, mean, or maximum).

| Snapshots | Label | Category | | Area | | | | AUC | |
| | | | | km^2 | | percent | | | |
		AUC	Sublethal Area	Sublethal	Hypoxic	Sublethal	Hypoxic	Sublethal	Hypoxic
1	Min-1	Min	Moderate	29,099	15,548	22.55	12.05	1.05	1.69
2	Min-2	Min	Moderate	29,465	15,460	22.83	11.98	1.05	1.69
3	Mean-1	Mean	Moderate	31,527	17,166	24.43	13.30	1.20	1.70
4	Mean-2	Mean	Moderate	31,951	17,341	24.76	13.44	1.20	1.68
5	Min-1	Mean	High	38,813	19,752	30.08	15.31	1.04	1.52
6	Min-2	Mean	High	38,667	19,869	29.96	15.4	1.04	1.51
7	Mean	Mean	High	38,083	16,972	29.51	13.15	1.19	1.80
8	Max	Mean	High	36,748	16,300	28.48	12.63	1.34	1.90

Table 2. Parameter values for the four movement algorithms used to simulate avoidance of low DO and the default behavior of individual fish.

Parameter	Value	Description	Equation(s)
ss_0	0.23	Baseline (default) swimming speed (m sec^{-1})	6, 8, 10
ϵ	0.9	Determines if wrapped Cauchy distribution is circular or ovoid	11
θ_m	0	Determines direction of bias of wrapped Cauchy distribution	11
util	2, 3, 1	Utility weight for NS, Sprint, and CCRW algorithms	14, 15, 16
mem	0.5, 0.5, 0.9	Memory weight for NS, Sprint, and CCRW algorithms	17, 18, 19
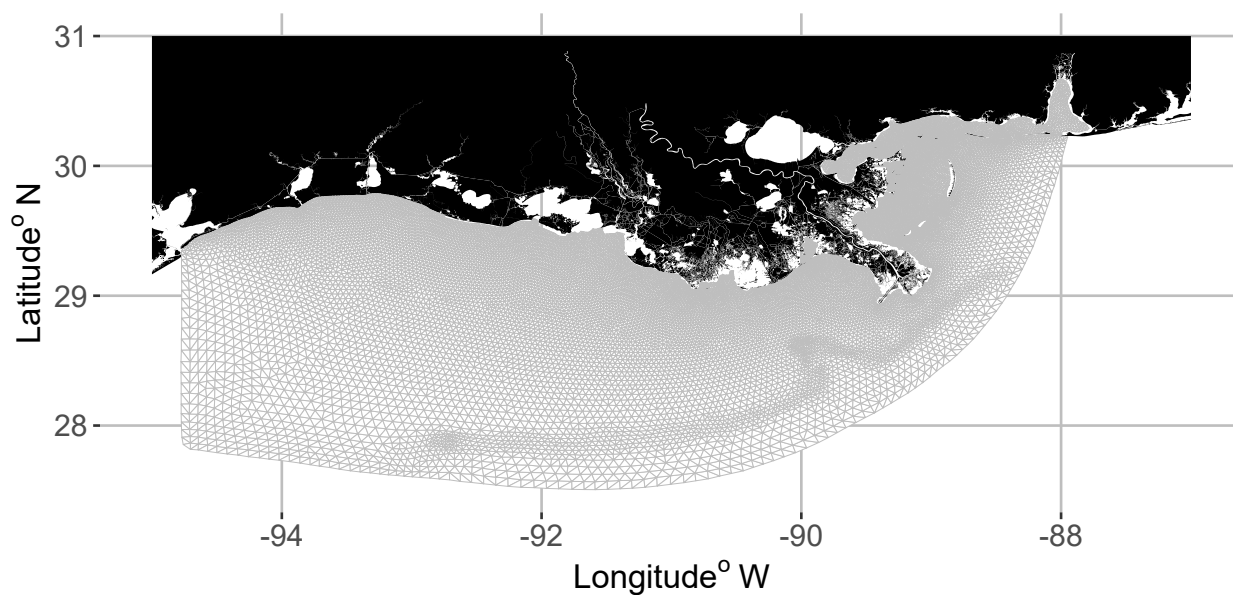
Figure 1. Planar view of the FVCOM-WASP model grid. There were also 30 vertical sigma layers.
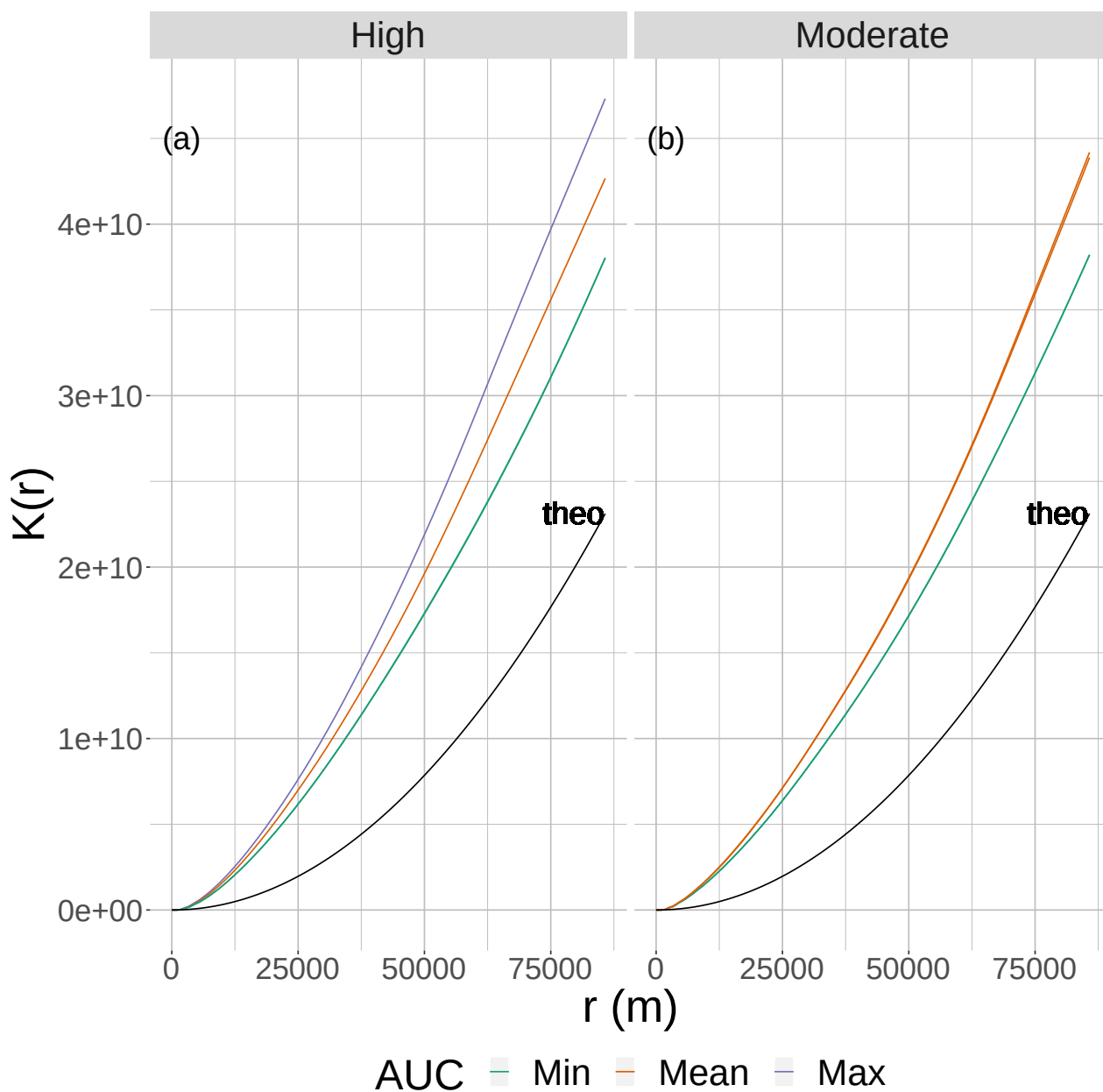
Figure 2. The results of Ripley's K function versus the neighborhood size (r) for eight static 2-D snapshot maps of DO from the bottom layer of the FVCOM-WASP simulation of 20–30 August 2002. The snapshots are defined in Table 1. Ripley's K values (lines) are shown for maps split into high (left) and moderate (right) sublethal areas, and by AUC values with each panel. There are lines for the two minimum and single mean and maximum AUC values for the high sublethal area, and for the minimum and to mean AUC areas for the moderate sublethal area. Some of the curves overlap and are not easily distinguished. The line labeled theo represents the relationship between Ripley's K and r for the theoretical condition when the spatial variability in sublethal DO cells is homogeneous.
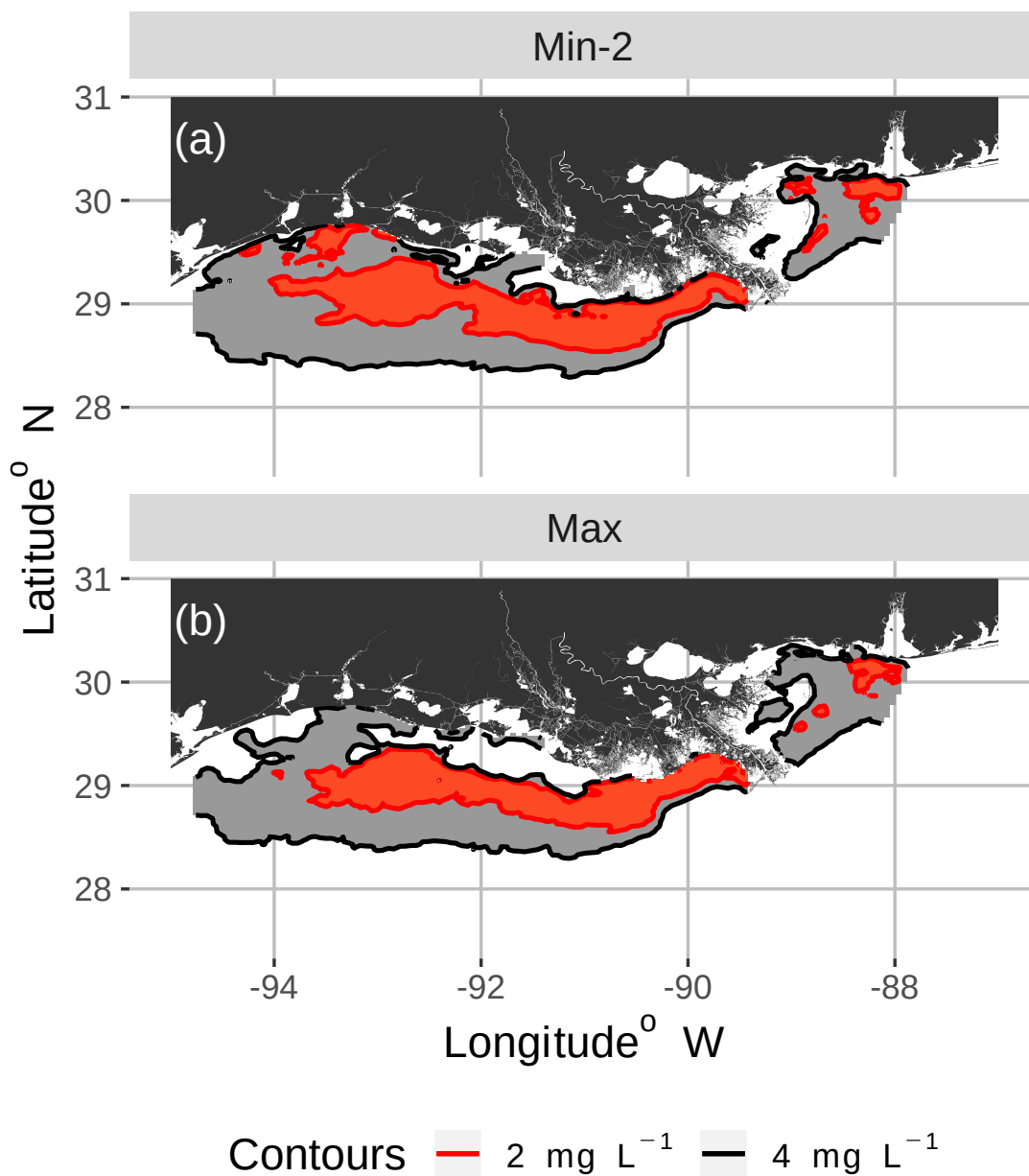
Figure 3. Spatial maps of bottom DO showing the 2 and 4 mg L^{-1} contours for two of the 8 snapshots from the FVCOM-WASP simulation of 20–30 August 2002. The snapshots are defined in Table 1. Snapshot Min-2 (top) is moderate sublethal area and minimum AUC, and snapshot Max (bottom) is high sublethal area and maximum AUC.
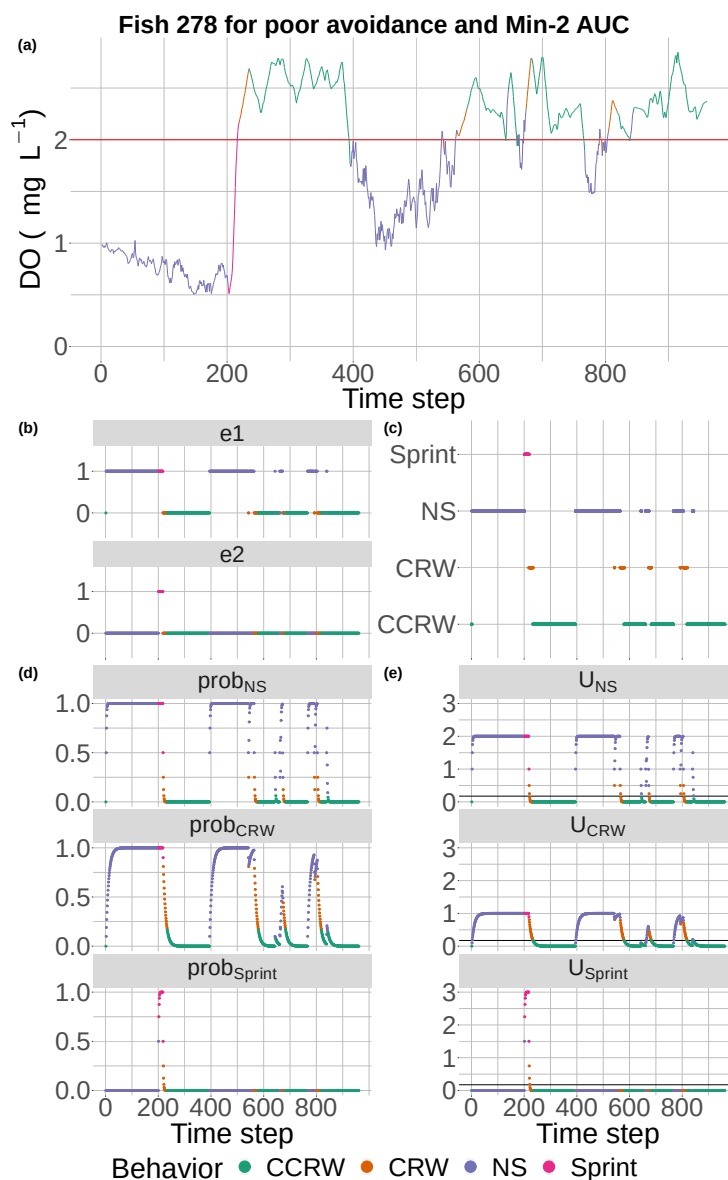
Figure 4. DO experienced and the component calculations used by the event based algorithm to select movement algorithms every 15 minute time step for fish 278 under the conditions of poor competency and one of minimum AUC (Min-2) maps with moderate sublethal area. DO is used each time step (panel a) to determine e1 and e2 (panel b), with e1 used to compute the probabilities for NS (tactical) and CRW (strategic) avoidance and e2 used to compute the probability for Sprint (panel d). These probabilities are used to compute utilities for the three algorithms each time step (panel e) and the algorithm with highest utility above a minimum threshold is selected to be used for movement for that time step (panel c). If none of the three avoidance-related algorithms are selected, then a fourth algorithm (CCRW) that is unrelated to DO concentration is used.
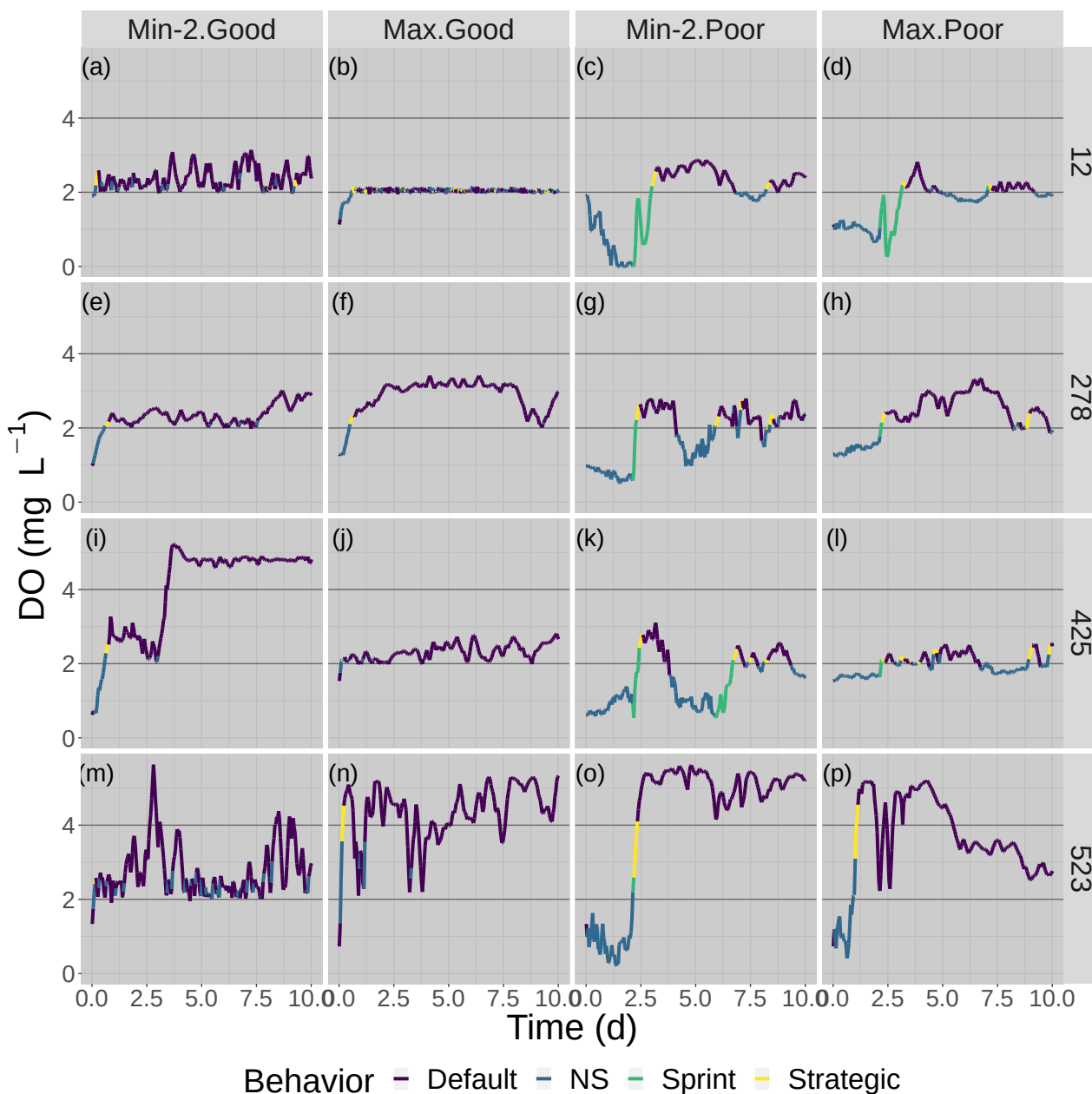
Figure 5. Time series of DO experienced by the four fish shown in Fig. 6 over the 10 days of the model for good and poor avoidance and the two snapshot DO maps (Min-2 for moderate sublethal and Max for high sublethal area). The color of the lines denotes the movement algorithm that each individuals was using. Black lines denote the thresholds for hypoxia (2 mg L^{-1}) and the upper value (4 mg L^{-1}) considered for sublethal concentrations.
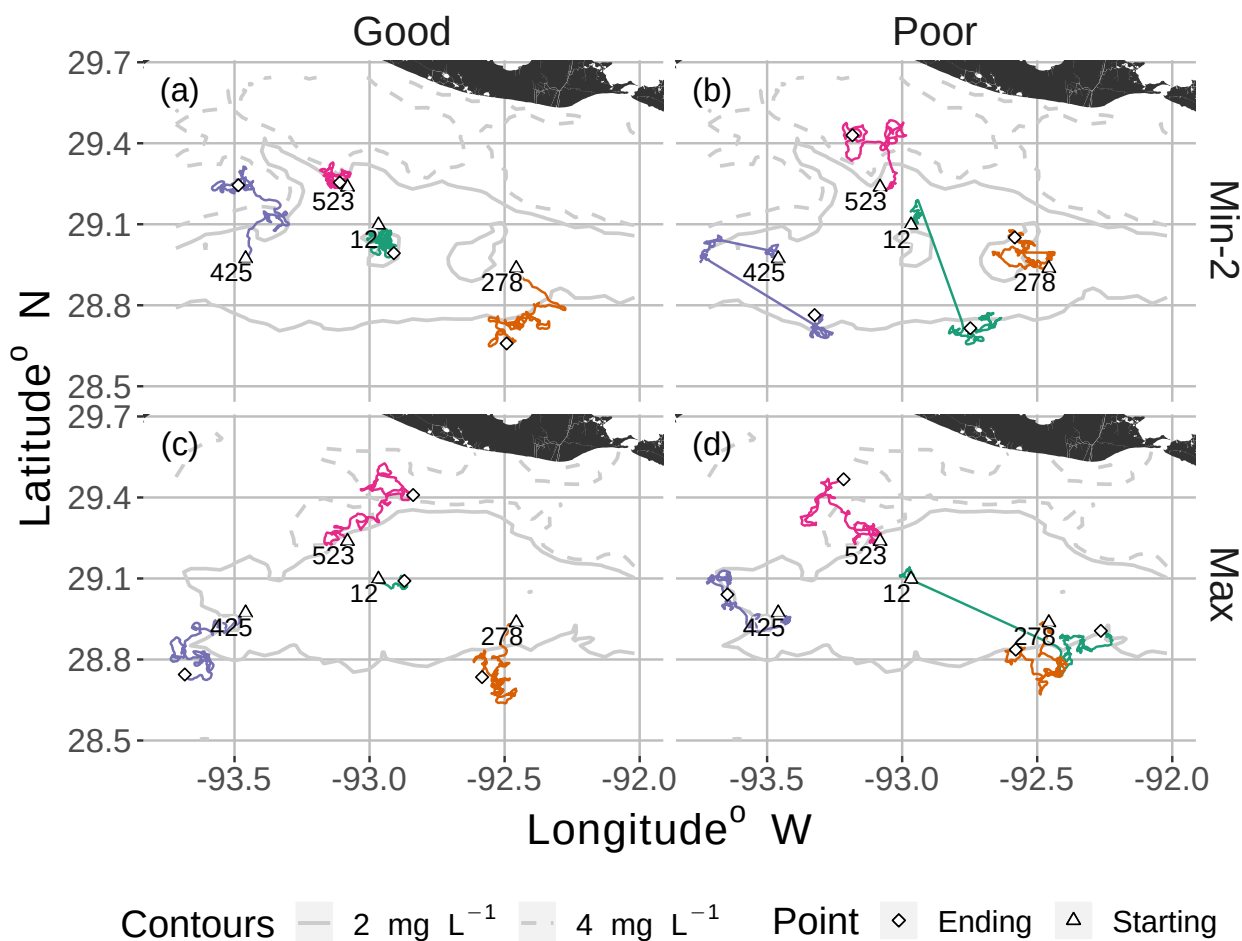
Figure 6. Movement tracks taken by four fish for good and poor hypoxia avoidance (left versus right) and two snapshots (Min-2 for moderate sublethal area and max AUC for high sublethal area). All four fish start (triangle symbol) in the hypoxic zone. These are the same maps as shown in Fig. 3, but only show a portion of the model grid.
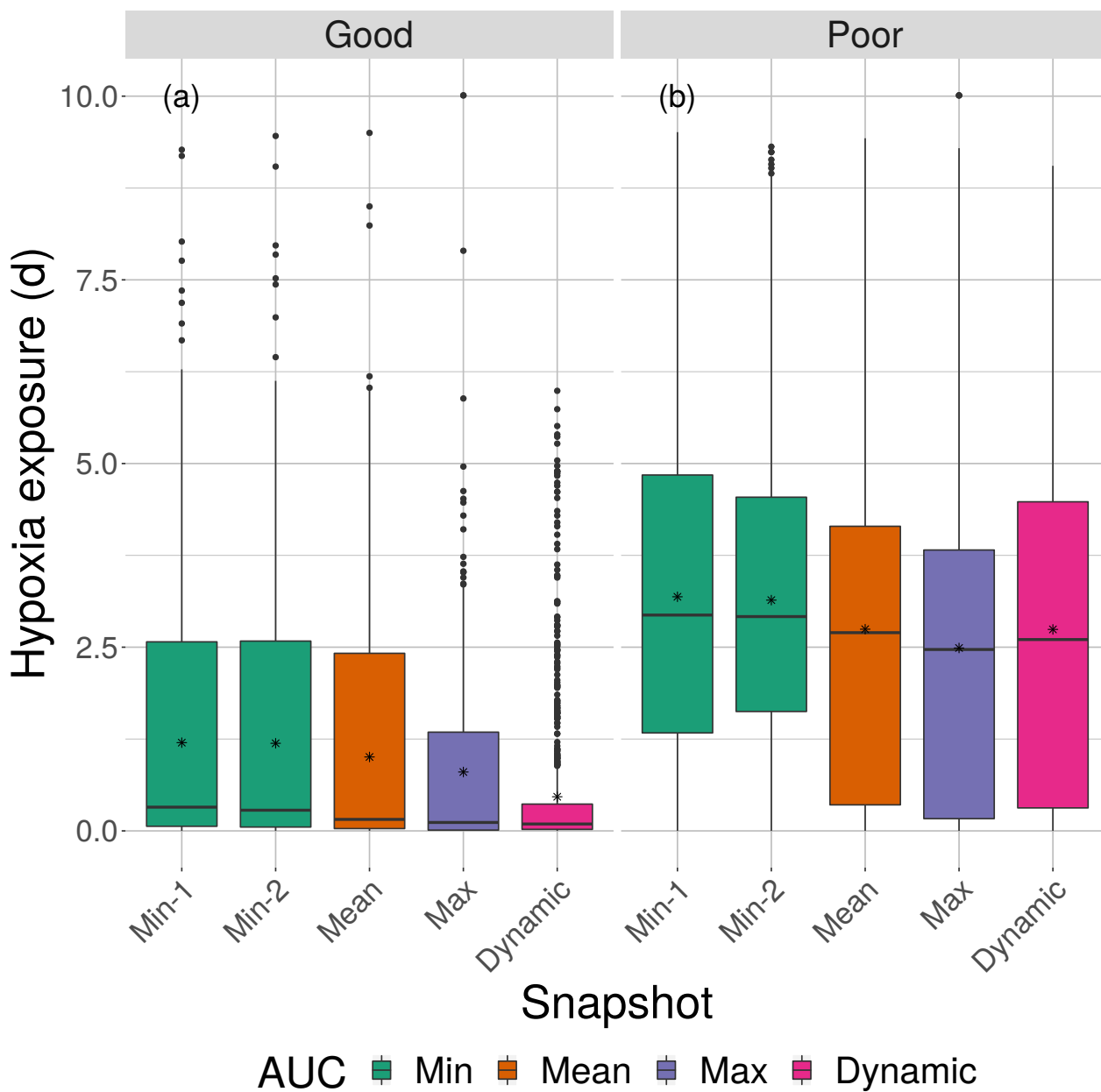
Figure 7. Boxplots of cumulative hypoxia exposure of all individuals (days) for good and poor competency on the four DO snapshot maps with high sublethal area. The cumulative exposure for the simulation using the dynamic map is also shown. The lower and upper lines of the boxplots show the 25th and 75th percentile value of cumulative exposure and the center line is the median. Individual fish values flagged as extreme values are shown as individual points. The star symbol denotes the mean.
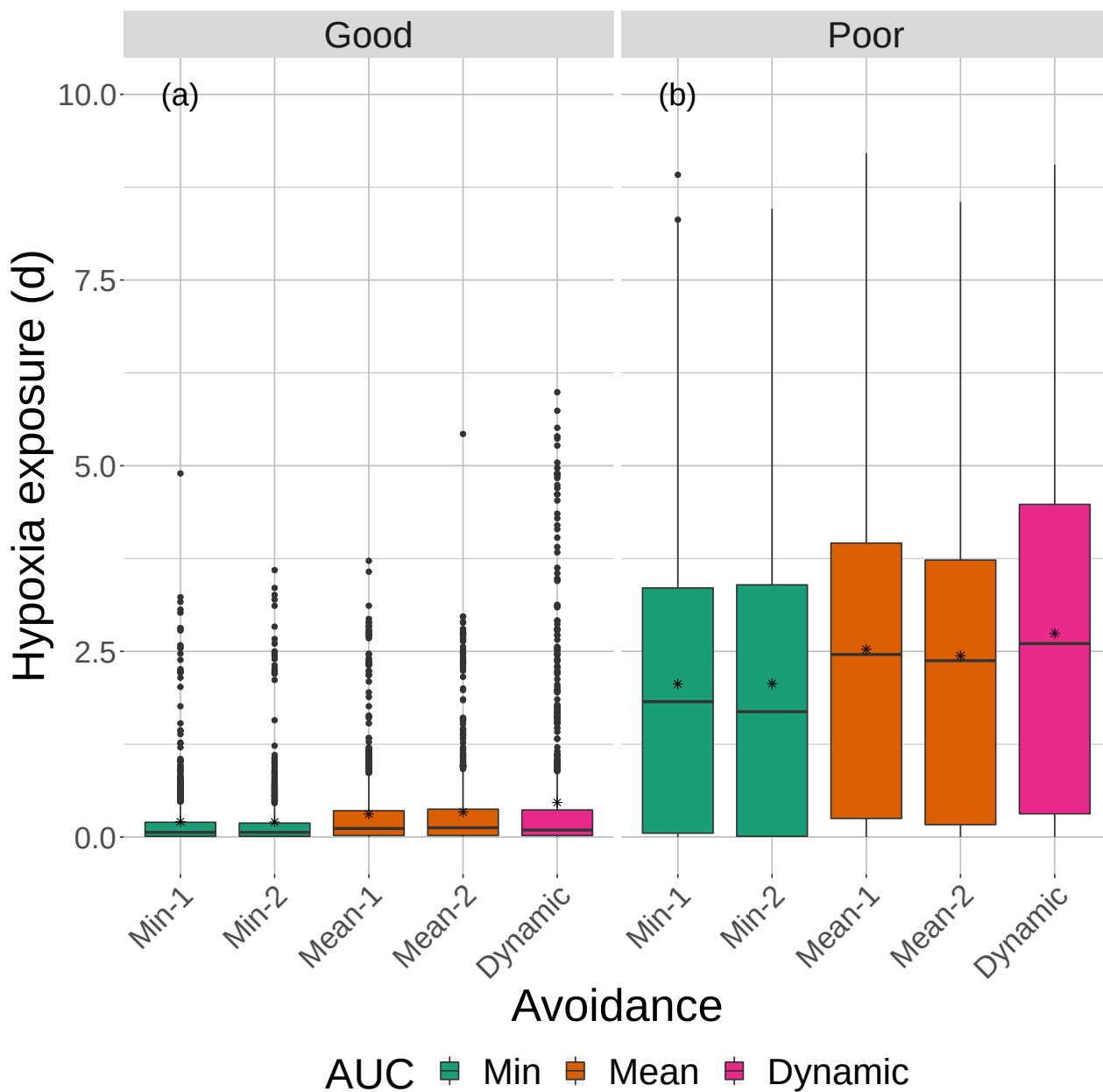
Figure 8. Boxplots of cumulative hypoxia exposure of all individuals (days) for good and poor competency on the four snapshot DO maps with moderate sublethal area. The cumulative exposure for the simulation using the dynamic map is also shown. The lower and upper lines of the boxplots show the 25th and 75th percentile value of cumulative exposure and the center line is the median. Individual fish values flagged as extreme values are shown as individual points. The star symbol denotes the mean.
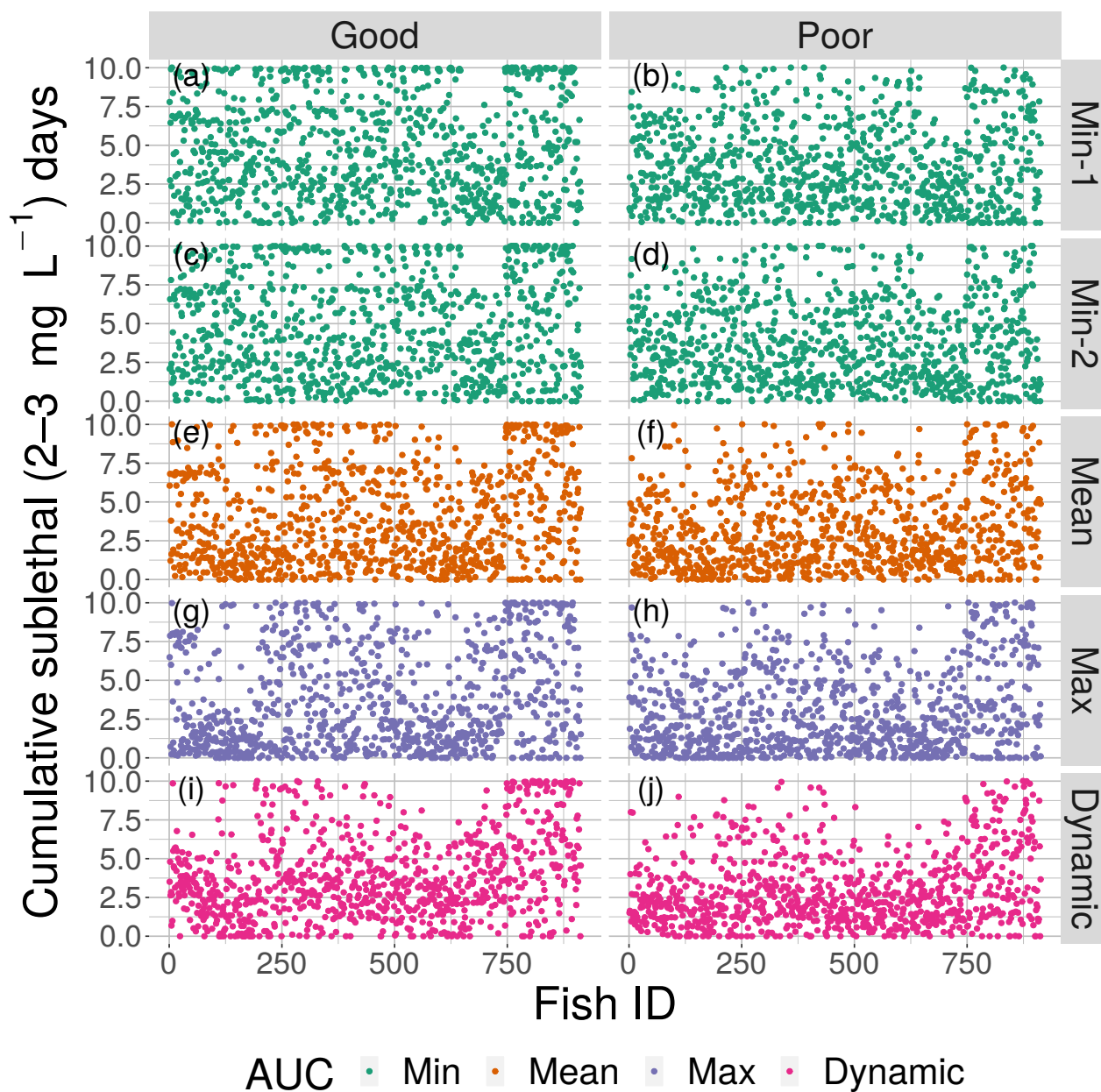
Figure 9. Cumulative exposure (days) of each individual fish to DO concentrations of 2–3 mg L⁻¹ for good (left) and poor (right) competency for each of the four snapshot DO maps with high sublethal area and the dynamic version. Maps within the same AUC category (two min maps) are shown with the same color.
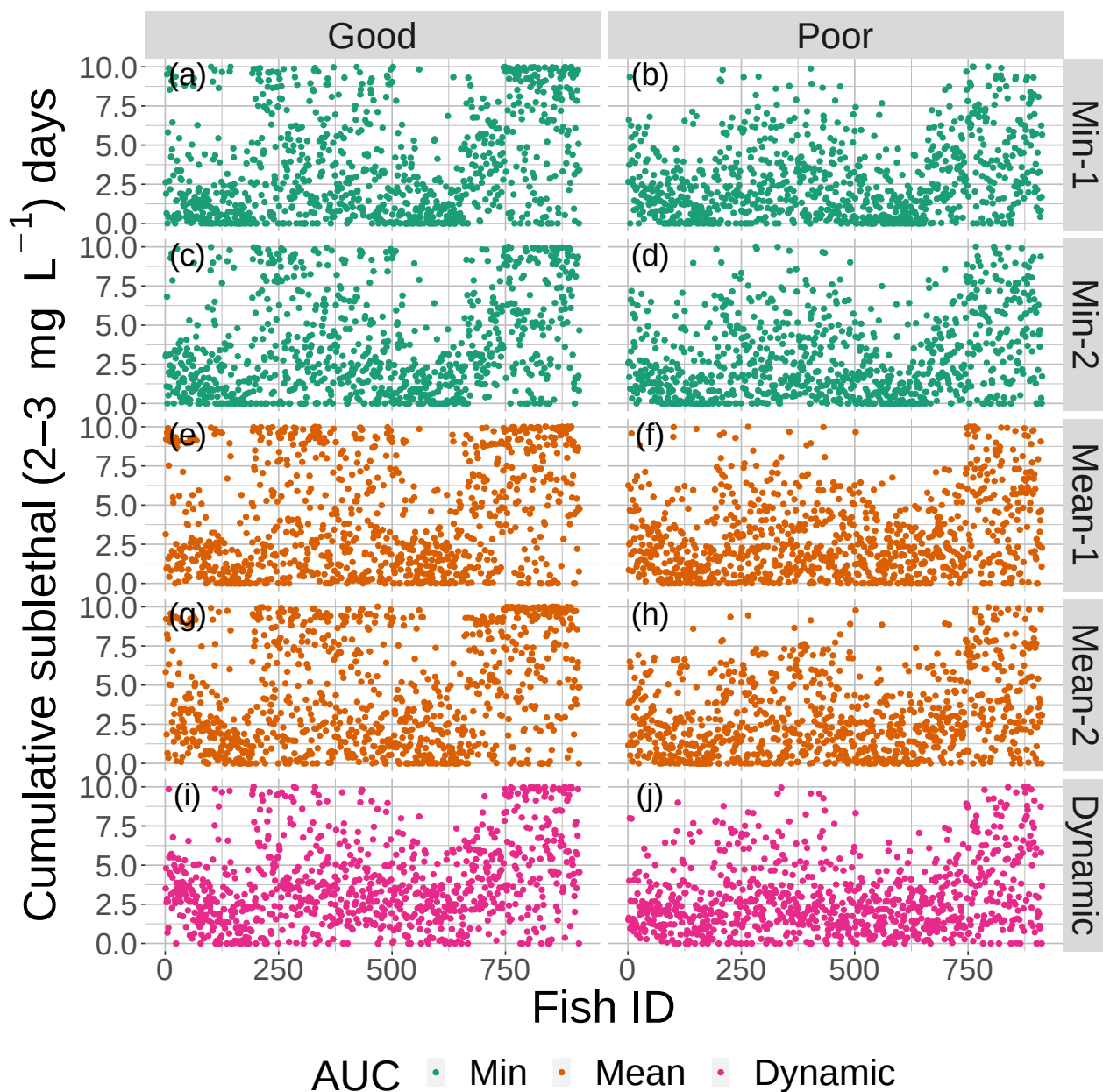
Figure 10. Cumulative exposure (days) of each individual fish to DO concentrations of 2–3 mg L^{-1} for good (left) and poor (right) competency for each of the four snapshot DO maps with moderate sublethal area and the dynamic version. Maps within the same AUC category (min and mean) are shown with the same color.
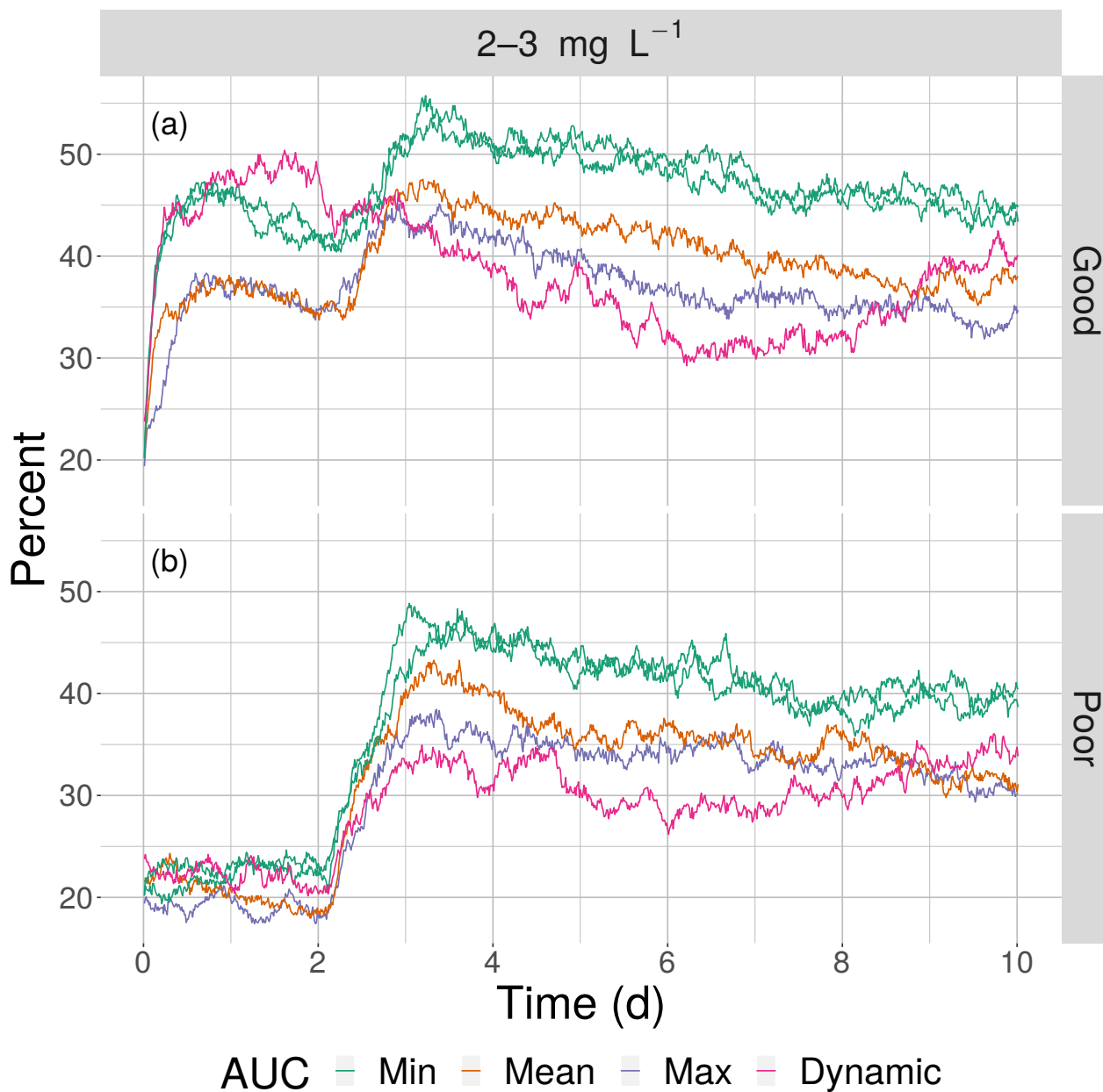
Figure 11. The percentage of fish exposed to DO of 2–3 mg L^{-1} for good (top) and poor (bottom) competency for the four snapshot maps with high sublethal area and the dynamic version. Maps within the same AUC category (min) are shown with the same color.
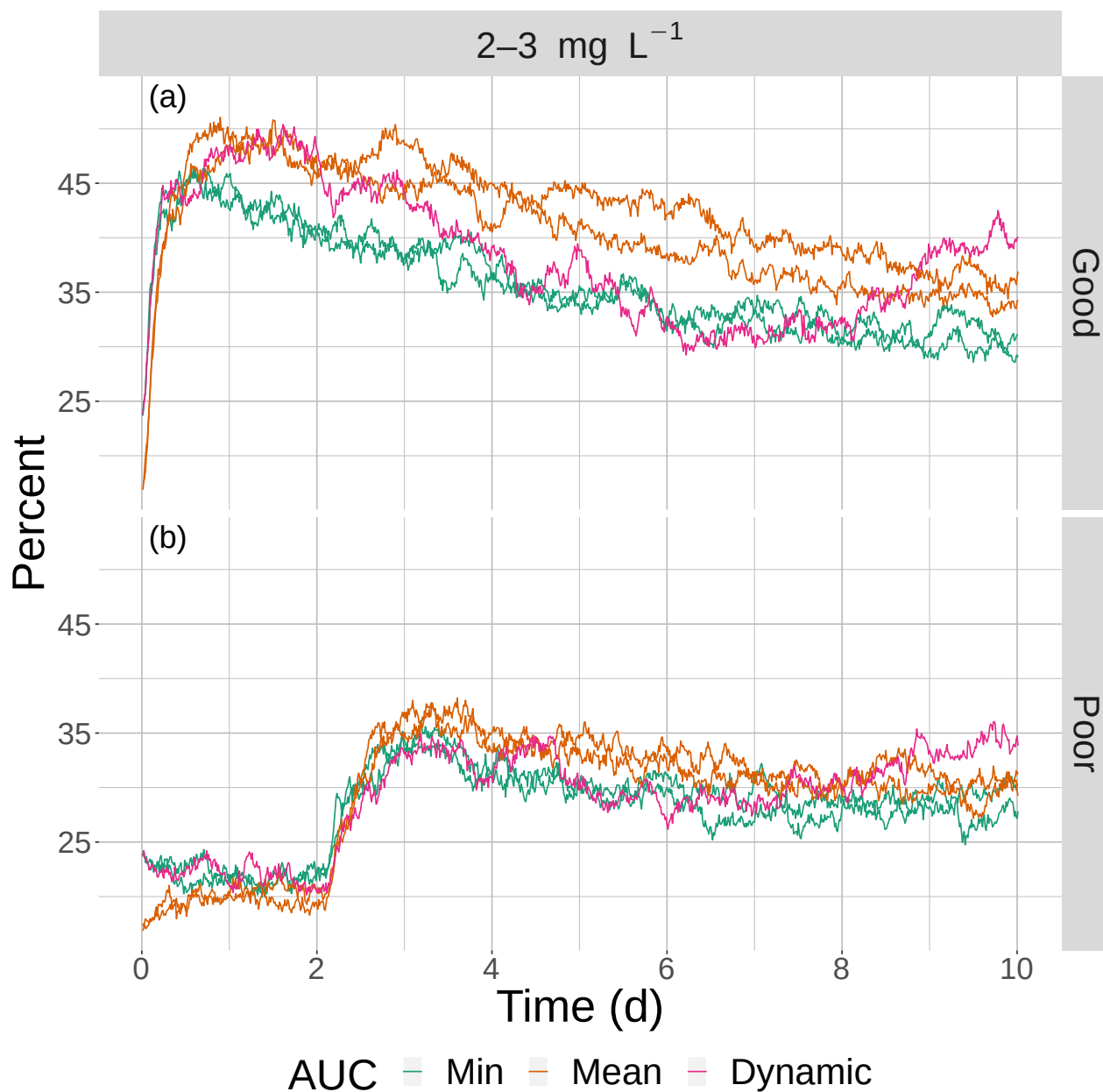
Figure 12. The percentage of fish exposed to DO of 2–3 mg L^{-1} for good (top) and poor (bottom) competency for the four snapshot maps with moderate sublethal area and the dynamic version. Maps within the same AUC category (min and max) are shown with the same color.